CHEMISTRY
A EUROPEAN JOURNAL

FULL PAPER

DOI: 10.1002/chem.201201180

Steric and Electronic Effects on the Configurational Stability of Residual Chiral Phosphorus-Centered Three-Bladed Propellers: Tris-aryl Phosphane Oxides

Tiziana Benincori,[a] Valentina Bonometti,[b] Roberto Cirilli,[c] Patrizia R. Mussini,[g] Andrea Marchesi,[d] Marco Pierini,[e] Tullio Pilati,[f] Simona Rizzo,*[f] and Francesco Sannicolò*[g]

Abstract: A series of tris-aryl phosphane oxides existing as residual enantiomers or diastereoisomers with substituents on the aryl rings differing in size and electronic properties were synthesized and characterized. Their electronic properties were evaluated on the basis of their electrochemical oxidation and reduction potentials together with those of the corresponding "blade bromides" (i.e., the naphthalene derivatives displaying the same substitution pattern of the tris-naphthyl phosphane oxide blades, with a bromo substituent where the phosphorus atom is located) determined by CV. The residual stereoisomeric phosphane oxides were isolated in a stereochemically pure state and were found to be highly configurationally stable at room temperature (stereoisomerization barriers of about 27 kcal mol^{-1}). The chiroptical properties of the residual stereoisomers and the assignments of absolute configuration are discussed. The configurational stability of residual tris-aryl phosphane oxides was found to be scarcely influenced by the electronic properties of the substituents present on the aromatic rings constituting the blades, while steric effects play the most relevant role. Detailed theoretical calculations are in agreement with the experimental results and also contribute to a rational interpretation of the stereodynamics of these systems.

Keywords: chirality · electrochemistry · phosphane oxides · residual stereoisomers · semiempirical calculations

Introduction

The stereodynamics of three-bladed molecular propellers is a fascinating research field currently attracting the interest of several renowned research groups.[1] It was investigated by Mislow et al. in the 1970s in the case of tris-aryl methanes[2] and tris-aryl amines[3] bearing three different aryl rings (denoted maximally labelled propellers). In the former case, in which the carbon atom located on the hub is a stereogenic center, two racemic diastereoisomers could be isolated, while in the latter two achiral diastereomers were separated, since fast pyramidal inversion removes nitrogen stereogenicity. This unusual form of stereoisomerism, which does not involve the presence of any rigid stereogenic element in the molecule, was named "residual" by Mislow et al.[2] In the case of tris-aryl methanes interconversion of the two diastereomeric residual racemates has a rather high barrier ($\Delta G^{\neq} \approx 30$ kcal mol^{-1} at 120 °C), while in the case of tris-aryl amines the diastereomerization process is much easier ($\Delta G^{\neq} \approx 18$ kcal mol^{-1} at −20 °C).

Differentiation of the edges of the blades and strict correlation of the motion of the rings are the prerequisites for the existence of residual stereoisomers in these systems. Residual stereoisomers result whenever closed subsets of appropriately substituted interconverting isomers (the residual stereoisomers) are generated from a full set of stereoisomers under the operation of a given stereoisomerization mecha-

[a] Prof. T. Benincori
Dipartimento di Scienza e Alta Tecnologia
Università dell'Insubria
via Valleggio 11, 22100 Como (Italy)

[b] Dr. V. Bonometti
Dipartimento di Chimica, Università degli Studi di Milano
via Golgi 19, 20133 Milano (Italy)

[c] Dr. R. Cirilli
Dipartimento del Farmaco, Istituto Superiore di Sanita′
Viale Regina Elena, 299, 00161 Roma (Italy)

[d] Dr. A. Marchesi
Laboratori Alchemia s.r.l.
via San Faustino, 68, 20134 Milano (Italy)

[e] Prof. M. Pierini
Dipartimento di Chimica e Tecnologie del Farmaco
Università di Roma "La Sapienza"
P.le Aldo Moro 5, 00185 Roma (Italy)

[f] Dr. T. Pilati, Dr. S. Rizzo
Istituto di Scienze e Tecnologie Molecolari
Consiglio Nazionale delle Ricerche
via Golgi 19, 20133 Milano (Italy)
E-mail: simona.rizzo@istm.cnr.it

[g] Prof. P. R. Mussini, Prof. F. Sannicolò
Dipartimento di Chimica and C.I.MA.I.NA
Università degli Studi di Milano
via Golgi 19, 20133 Milano (Italy)
Fax: (+39) 02-50314139
E-mail: francesco.sannicolo@unimi.it

Supporting information for this article is available on the WWW under http://dx.doi.org/10.1002/chem.201201180.

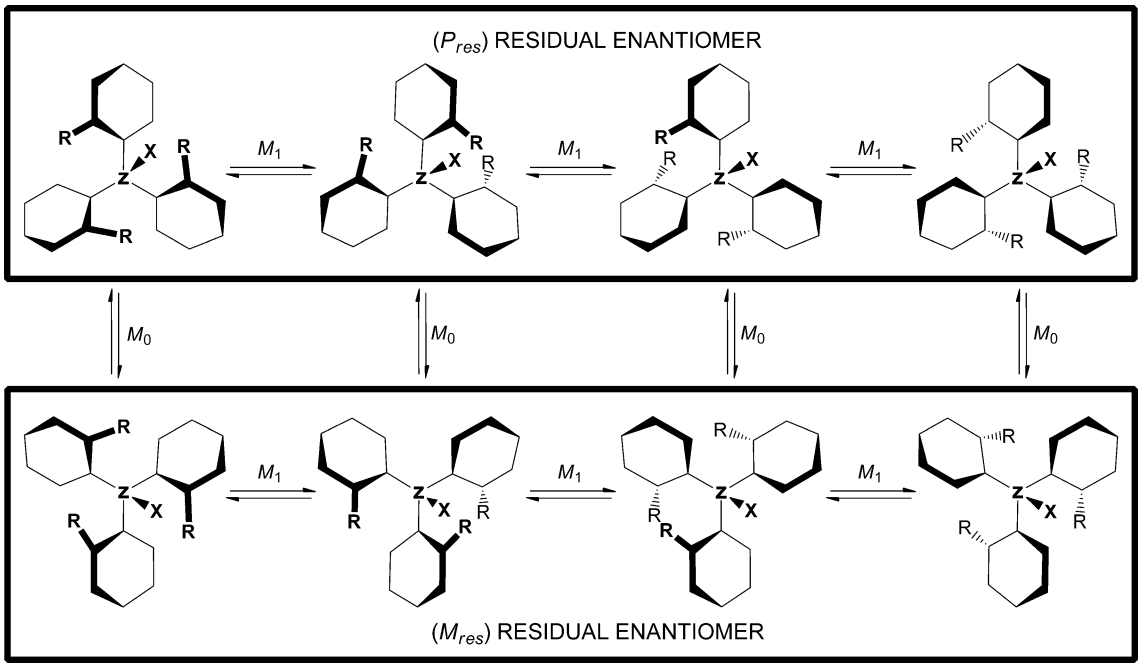

Figure 1. Stereodynamic sequence of three-bladed propeller-shaped molecules bearing identical blades (see text for discussion). The enantiomorphism of each stereoisomer pair resulting from the M_0 mechanism has been visually enhanced by adding a 60° rotation around the C_3 axis.

nism. Helicity reversal (the so-called M_0 mechanism, Figure 1) is not the fastest stereoisomerization process for three-bladed propellers displaying correlated rotation of the rings, as commonly believed, and the two-ring flip mechanism (the so-called M_1 mechanism, Figure 1) is the lowest energy process. It does not interconvert all eight possible conformational stereoisomers generated by helicity and the three simple blade-hub rotors. In the case of systems bearing three identical blades, two non-interconverting subgroups in an enantiomeric relationship (the residual enantiomers, framed in Figure 1) are generated, each one constituted by four quickly interconverting diastereoisomers.[4] The M_1 mechanism is fast at room temperature, involving barriers of about 10 kcal mol^{-1}, while the energy required for interconversion of the residual stereoisomers corresponds to that controlling the M_0 mechanism. If this barrier is higher than 20 kcal mol^{-1}, the residual stereoisomers should be configurationally stable enough to be separated in a stereoisomerically pure state.

We have focused our recent attention on phosphorus-centered C_3 propellers,[5,6,7] since access to a unconventional class of chiral tris-aryl phosphanes as ligands for transition metals in homogeneous stereoselective catalysis appeared to be an exciting challenge, particularly considering that hindered tris-aryl phosphanes are the promoters of choice in several metal-catalyzed reactions.[8]

We recently reported the synthesis, structural characterization, and resolution of phosphane oxides **1** and **7**.[6] We were able to assign the absolute configuration to the residual antipodes of **7** by anomalous X-ray scattering and, by correlative methods, to all other residual enantiomers, both carbon- and phosphorus-centered, known so far, and they display configurational stability high enough to allow their survival during resolution by HPLC on a chiral stationary phase (CSP). We also coined configurational descriptors for the residual enantiomers of three-bladed propellers. We suggested to assign to a given residual enantiomer the configurational descriptor P_{res} or M_{res} (res = residual) according to the helix exhibited by the diastereoisomer of each subset having the prioritary edges of the blades above the reference plane, which is the plane defined by the three atoms connected to the hub (Figure 1).[6]

The primary aim of this work was to investigate the steric and electronic effects of the substituents present on the blades on the configurational stability of phosphorus-centered propellers, phosphane oxides in particular, existing as residual stereoisomers. To evaluate the electronic effects, the obvious strategy was to synthesize a series of new compounds, derived from **1** and **7**, bearing electron-withdrawing (nitro, sulfo, bromo) or electron-releasing (ethoxyl) groups in selected positions of the naphthalene rings not involved in the dynamic gearing of the blades (Figure 2).

To investigate the steric effects, we resorted to substrates **10** and **11** (Figure 2). Phosphane oxide **10** was designed according to the following rationale: 1) At least one of the two methyl groups on the dioxene ring is located in the center of the gearbox controlling the correlated rotation of the blades. 2) The carbon atoms bearing the methyl groups are stereocenters that all display the same *S* configuration. Their stereogenicity combined with residual stereogenicity implies that two residual diastereoisomers are produced, distinguishable (^{1}H and ^{31}P NMR spectroscopy) and separable by achiral techniques (chromatography on an achiral SP). 3) The methyl groups are forced to stay equatorial and thus

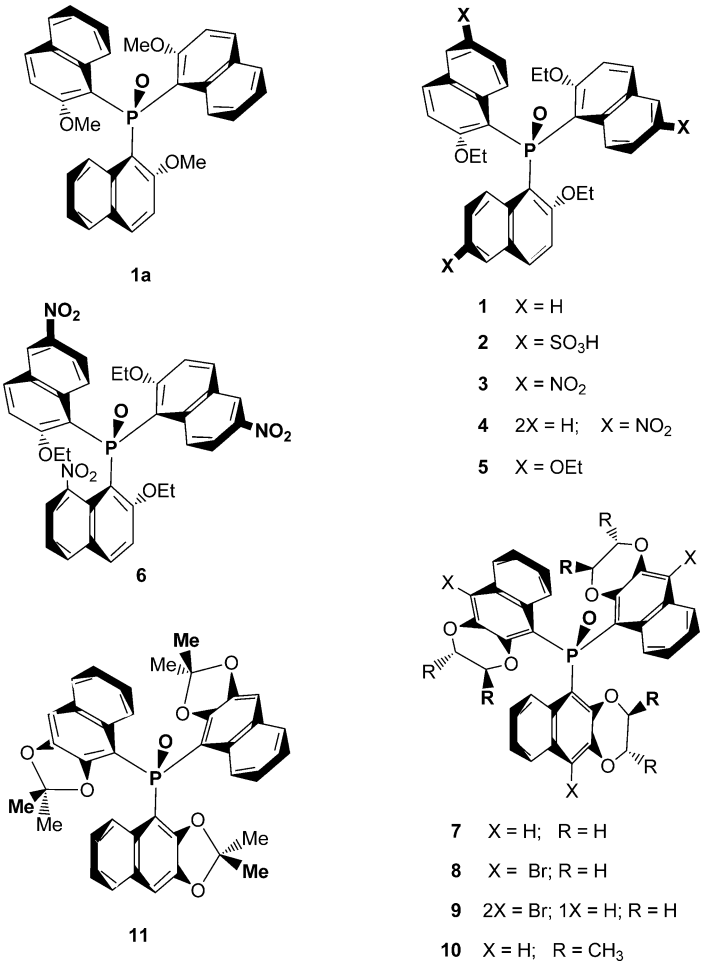

Figure 2. The series of phosphane oxides considered in the present work.

block dioxene ring flipping, which in **7** overlaps with the residual stereoisomerism dynamics and makes interpretation of the dynamic NMR data unreliable.

Phosphane oxide **11** is characterized by a 2,2-dimethyl-1,3-dioxolene ring fused to the naphthalene unit constituting the blade; the steric hindrance of the five-membered ring is smaller than that associated with the 1,4-dioxane ring, and the methyl groups above and below the plane of the blade appear less efficient than the methyl group in the 2-position of the naphthodioxene ring in **10** in promoting correlated rotation of the rings. Furthermore, the behavior of C_1-symmetric trinitro phosphane oxide **6**, carrying one nitro group in a very critical position for interfering with the mechanical gearing of the blades, could add some additional information on the effects of stereoelectronic factors on the configurational stability of residual stereoisomers.

Results and Discussion

Synthesis of the substrates: Phosphane oxides **1** and **7** (and the corresponding phosphanes) were described by us previously.[6] Treatment of a solution of the phosphane corresponding to **1** in chloroform with a 65% aqueous nitric acid solution under vigorous stirring at 50°C afforded a complex mixture of products, three of which were separated and isolated in a pure state by silica-gel column chromatography. Phosphorus oxidation expectedly occurred during the nitration process. Product **3** results from nitration in the 6-position of all naphthalene rings of the phosphane corresponding to **1**, while **6** is a constitutional isomer of **3** bearing a nitro group in the 8-position of a single naphthalene moiety. Direct nitration of phosphane oxide **1** gave less satisfactory results. The structures of these products have been univocally confirmed by analytical and spectral data and by single-crystal X-ray diffraction analysis (see below). The C_1-symmetric mononitration product **4**, bearing the nitro group in the 6-position of one naphthalene ring, was isolated. Structural assignment is based on univocal interpretation of MS and NMR data.

Bromination of phosphane oxide **7** with *N*-bromosuccinimide (NBS) in 50% acetic acid/chloroform solvent afforded phosphane oxides **8**, as the main product and **9**, as a by-product. Structural assignment to these products is based on the univocal interpretation of MS and NMR data.

Phosphane oxides **1a**, **2**, **5**, **10**, and **11** were quantitatively obtained by oxidation of the corresponding phosphanes with an excess of hydrogen peroxide.[9] A diastereomeric mixture of **10** was obtained by oxidation of a diastereomeric mixture of the corresponding phosphanes with hydrogen peroxide. The two residual diastereoisomers were separated on a preparative scale by silica-gel column chromatography or by HPLC on a CSP on a semi-preparative level (see below). Crystallization of phosphane oxide **11** as a conglomerate from ethyl acetate allowed the spontaneous resolution process (see below).

X-ray diffraction data: The crystal structures of **1** and **7** were reported by us previously.[6] The structural assignments to some of the phosphane oxides described in this paper, namely, **1a**, **3**, **6**, **10**, and **11** were confirmed by the X-ray diffraction data (Figure 3).

An abnormal distortion of the naphthalene ring bearing the nitro group in the 8-position is clearly visible in the structure of **6**. It is associated with an anomalous loss of coplanarity, and therefore in conjugation, between the aromatic ring plane and that of the nitro group, which diverge by about 40°, whereas a maximum of 10° is observed in the other two 6-nitro-substituted rings and in all blades of **3**. This anomalous situation is probably produced by the strong steric interactions occurring between the *peri* nitro group and the oxygen atom of the adjacent phosphane oxide group.

The C-P-C angles in **11** [112.34(4)°], which displays crystallographic C_3 symmetry, are surprisingly greater than those found in the crystal structure of **1a** (109.57(13)°) and suggest strong steric interference amongst the blades of the propeller and hence more efficient blade gearing.

Resolution of the residual racemates of phosphane oxides 1, 3–9, and 11 and separation of the residual diastereoisomers

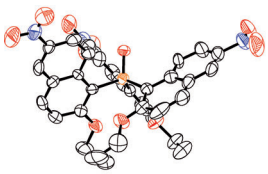

(M_{res})–**3** [and (P_{res})–**3**]

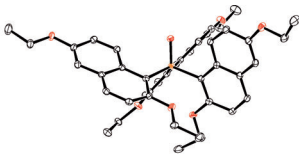

(M_{res})–**5** [and (P_{res})–**5**]

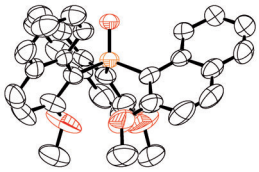

(M_{res})–**1a**

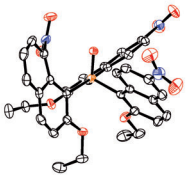

(+) – (P_{res})–**6**

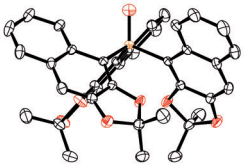

(+) – (P_{res})–**11**

Figure 3. ORTEPs of (±)-**3** and (±)-**5**: only one enantiomer is shown even though both enantiomers are present in the crystal. Only one enantiomer is present in the crystal of **6** (racemate resolved by CSP HPLC), **1a**, and **11** (conglomerates), whereby the P_{res} enantiomer corresponds to the dextrorotatory antipode. Hydrogen atoms are omitted.

of 10: We previously demonstrated that residual phosphane oxides are in general configurationally stable enough to be separated as enantiopure antipodes at room temperature.[6,7] The availability of enantiopure samples of the stereoisomers of the different compounds is essential for acquiring their chiroptical properties, which are very useful tools to assign the absolute configuration to them by correlative methods. The residual racemates of all phosphane oxides, except for **2**, were effectively resolved by analytical or semi-preparative HPLC on the immobilized-type Chiralpak IC CSP.[10] The reversed-phase HPLC resolution experiments on racemic trisulfonic acid **2** were unsuccessful, while direct-phase resolution attempts were promising albeit complicated by the extremely low solubility of the compound in the solvents usually employed for this purpose (see Supporting Information).

Even though the resolution of the racemates of **1** and **7** was already described by us in a previous paper,[6] we considered it worth carrying out all of the chromatographic resolution experiments under very similar, if not identical, conditions so as to have a reliable elution order for the antipodes. Resolution was excellent in all cases (see Supporting Information) and several milligrams of each enantiomer of **1**, **3**–**9**, and **11** were obtained in a pure state. As anticipated, pure samples of both antipodes of **11** and of the diastereoisomers of **10** were obtained by spontaneous resolution and by silica-gel column chromatography, respectively.

Typical chromatograms illustrating the baseline enantioseparation of **4**, **8**, and **11**, recorded with dual UV/CD detection are shown in Figure 4. The specific rotations of the enantiomers of the phosphane oxides, the chromatographic retention factors ($k_{1,2}$), the enantiomeric excesses of the resolved antipodes, and their absolute configuration, assigned by comparison of the CD spectra (see below) are summarized in Table 1.

The big difference in the absolute value of the specific rotation of the two diastereoisomers of **10** is due to the contributions of the stereogenic elements in the molecules, which are synergic in the first-eluted and opposite in the second-eluted stereoisomer, that is, the helicity, which is opposite in

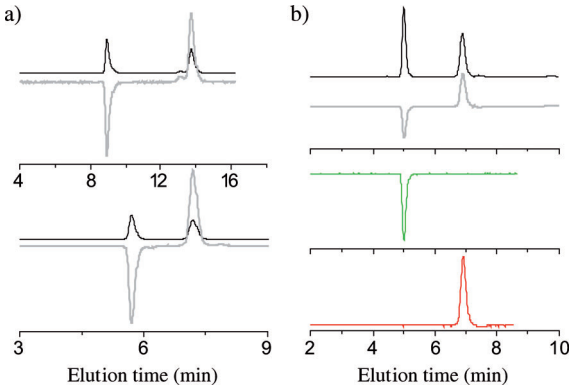

Figure 4. a) Chromatograms of the racemate of tribromo derivative **8** (top) and of mono-nitro derivative **4** (bottom), recorded by simultaneous on-line CD (gray line) and UV (black line) detection at 254 nm; eluent: *n*-hexane/dichloromethane/ethanol (65/35/1) (top) and dichloromethane/methanol (100/1) (bottom); flow rate: 1.0 mL min^{-1}; temperature: 25 °C. b) Chromatograms of the racemic mixture of **11** and of pure enantiomers obtained from the chromatographic separations. Column: Chiralpak IC (250 mm × 4.6 mm I.D.); eluent: *n*-hexane/dichloromethane/ethanol 20/100/1; flow rate: 1.0 mL min^{-1}; temperature: 25 °C; detection, UV (black line) and CD (gray, green, and red lines) at 254 nm.

Table 1. Specific rotation, retention factor (k), enantiomeric excess, and absolute configuration (AC) of the resolved stereoisomers of phosphane oxides.

Compound	First-eluted residual stereoisomer			Second-eluted residual stereoisomer		
	k_1 (AC)[a]	*ee* [%]	[α][b]	k_2 (AC)[a]	*ee* [%]	[α][b]
1a	0.83 (M_{res})	>99	−459	1.12 (P_{res})	>99	+458
1	1.25 (M_{res})	>99	−487	1.48 (P_{res})	>99	+485
3	0.80 (M_{res})	>99	−820	1.08 (P_{res})	>99	+810
4	0.90 (M_{res})	>99	−504	1.55(P_{res})	>99	+504
5	1.05 (M_{res})	>99	–[d]	2.06 (P_{res})	>99	(+)[d]
6	0.98 (M_{res})	>99	−765	1.46 (P_{res})	>99	+763
7	0.97 (M_{res})	>99	−445[c]	1.23 (P_{res})	98	+443[c]
8	1.98 (M_{res})	>99	−351	3.57 (P_{res})	>99	+345
9	0.55 (M_{res})	>99	−331	0.93 (P_{res})	>99	+326
10	1.15 (M_{res})	>99 (*de*)	−282	2.16(P_{res})	99 (*de*)	+5
11	1.67 (M_{res})	>99	−320	1.30 (P_{res})	>99	+321

[a] Absolute configuration. [b] $c = 0.1\%$ in $CHCl_3$. [c] $c = 1\%$ in CH_2Cl_2. [d] Sign of optical rotation monitored on-line at 365 nm during enantioselective HPLC.

the two stereoisomers, and the six carbon stereocenters, which have identical configuration in both compounds.

Circular dicroism spectra of residual antipodes and diastereoisomers 10 and correlative configurational assignment: The CD spectra of the residual antipodes of all phosphane oxides, except for **2**, whose racemate was not resolved, and those of the two diastereoisomers of **10** are shown in Figure 5. The CD behavior of all residual stereoisomers is

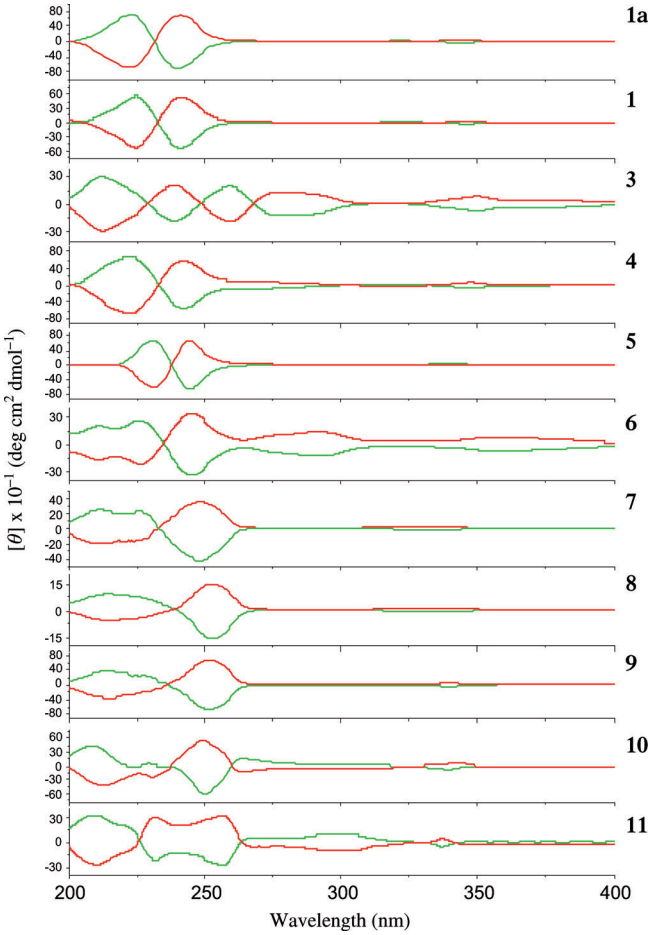

Figure 5. CD spectra of the resolved residual enantiomeric and diastereomeric (**10**) phosphane oxides in 0.1–0.2 mg mL^{-1} acetonitrile solution. Green curves refer to the levorotatory, first-eluted, M_{res} stereoisomers and the red curves to the dextrorotatory, second-eluted, P_{res} stereoisomers.

quite similar: the spectra of all the first-eluted products (all levorotatory, as anticipated) display the first bisignate curve above 200 nm, characterized by a negative Cotton effect. All of them should have M_{res} absolute configuration, since M_{res} configurations of (−)-**3**, and (−)-**7** were demonstrated by single-crystal X-ray anomalous diffraction data (Figure 3).[6] We verified that all the residual enantiomers display CD curves which are perfect mirror images and thus all dextrorotatory antipodes have the P_{res} absolute configuration.

The CD spectra of the two diastereoisomers of **10** deserve special comment. They display quasi-enantiomorphic curves. This observation confirms that the contribution to the CD properties of the helicity exhibited by the most stable conformer of the four constituting the residual diastereoisomers (Figure 1), which is also that present in the crystal, with the prioritary edges of all the blades *anti* (*aaa*) with respect to the oxygen atom of the PO group, is much more important than the effect of the six homomorphic rigid stereogenic centers present on the three blades.

Helix inversion barriers of the residual stereoisomers of phosphane oxides: The helix inversion barriers related to activation of the M_0 mechanism were evaluated by two different approaches: classical off-column kinetic studies combined with enantio- or diastereoselective HPLC and dynamic ^{1}H NMR spectroscopy. Off-column stereoisomerization kinetics studies were performed on a single enantiomer in $CHCl_3$ solution at 55 °C. The ^{1}H NMR technique was necessarily employed in the case of phosphane oxide **2**, which was not obtained in an enantiomerically enriched state: the behavior of the methylene hydrogen signals of the ethoxyl groups was examined at different temperatures.

In the case of the residual M_{res} and P_{res} diastereoisomers **10**, for which the removal of residual stereogenicity through the M_0 mechanism would produce a single classical enantiomer, two barriers are expected. They were evaluated by off-column diastereomerization experiments carried out on each of the two residual diastereoisomers previously resolved by semipreparative chromatography in a highly enriched diastereomeric state.

Graphical examples of the two techniques are given for the case of **11** in the off-column kinetics studies (Figure 6a) and for the case of **2** for the ^{1}H DNMR experiments (Figure 6b). The enantiomerization and diastereomerization rate constants and the corresponding energy barriers ($\Delta G^{\neq}$) are reported in Table 2. They demonstrate that all of the phosphane oxides display a quite high configurational stability, since the energy barriers to be surmounted for activating helix reversal through the M_0 mechanism are quite high. The residual stereoisomers of these compounds could be stored in a fridge in a stereomerically pure state for years.

The second observation is that steric factors, such as the dimensions and rigidity of the dioxolene and dioxene condensed rings, exert a relevant influence on the configurational stability of this kind of stereoisomers. Substrates **6**, **10**, and **11**, displaying a substitution pattern which directly affects the dynamic gearing of the blades, exhibit helix inversion barriers which mostly differ from the average value of 27.0–28.6 kcal mol^{-1} shown by the other phosphane oxides, in which only classical electronic effects are expected. The most sterically hindered substrates **10** are the configurationally most stable stereoisomers, displaying a helix inversion barrier about 2 kcal mol^{-1} higher than that shown by the less encumbered parent compound **7**. The opposite behavior is shown by compound **11**, in which the presence of a condensed five-membered ring reduces the helix inver-

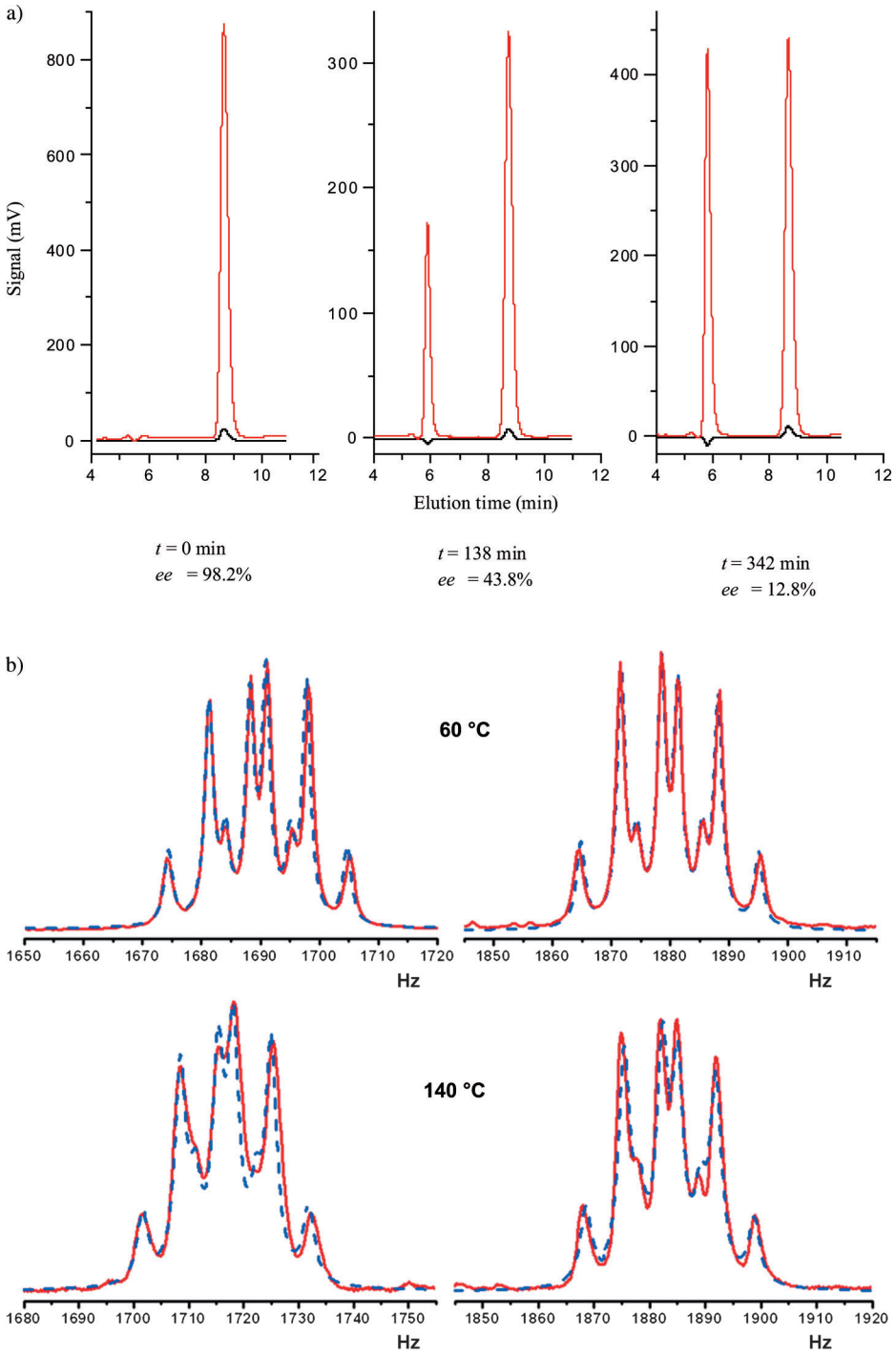

Figure 6. a) Off column racemization of (+)-**11**; $CHCl_3$, 55 °C; CSP column: Chiralpak IC 250×4.6 mm I.D.; eluent: *n*-hexane/CH_2Cl_2/EtOH 20/100/1; flow rate: 1.0 mL min^{-1}; 25 °C; detection: UV (black line) and CD (gray line) at 254 nm. b) ^{1}H DNMR spectrum of **2** ([D_6]DMSO): methylene group signals; spectra refer to the frozen (above) and active (below) enantiomerization process (continuous red line corresponds to experimental and dashed blue line to simulated spectra).

sion barrier by up to 2 kcal mol^{-1} with respect to the average value.

Table 2 also shows quite modest differences in the barriers shown by all of the other phosphane oxides, even though their substitution patterns are very different. In fact, in the two subensembles of compounds **1–5** (**SE$_1$**) and **7–9** (**SE$_2$**), in which electronic contributions more than steric hindrance should be considered significant for influencing the helix inversion rate, the maximum variation of $\Delta G^{\neq}$ was found to be 1.6 and 0.4 kcal mol^{-1} respectively.

Theoretical investigation of electronic property–configurational stability relationships: Theoretical support for the electronic origin of these effects was sought by analyzing the extent of linear correlation between the helix reversal barriers and molecular descriptors of the electronic effects calculated on the ground state of all phosphane oxides **1–11** (details of the calculation procedure are given in the Experimental Section). The same calculation was also performed on tris(1-naphthyl)phosphane oxide (**M0**) as reference model.

Attention was preliminarily focused on the atomic charges located on phosphorus (δ_P) and oxygen (δ_O) atoms of the P=O group, as well as on the length of the P=O bond $d_{P=O}$ (Table S1 of Supporting Information). The choice of the first two descriptors was suggested by the knowledge that charges localized on acidic hydrogen atoms or on atoms carrying acidic hydrogen atoms, assessed by quantum mechanical calculations at either semi-empirical[11–19] or ab initio level,[11,20–26] are effective descriptors of acidity that can sensitively reflect even small conformational[16,17] and configurational[16–18,20] changes in the structure of the substrate. Interestingly, several examples[11,22–26] showed that improvements in the level of theory of the quantum mechanical methods used to assess the molecular descriptors (e.g., HF or DFT instead of semiempirical methods, as well as larger basis sets within HF or DFT approaches) do not necessarily lead to significant improve-

Table 2. Enantiomerization/diastereomerization rate constants (k_{rac}/k_{diast}) and energy barriers ($\Delta G^{\neq}$) for residual phosphane oxides.

Compound	k_{rac}/k_{diast} [s^{-1}]	$\Delta G^{\neq}$ [kcal mol^{-1}]	r^2	Method[a]
1	3.17×10^{-6}	27.53	0.9996	a
2	4.40×10^{-2}	27.0	–	b
3	2.08×10^{-6}	27.80	0.9998	a
4	3.24×10^{-6}	27.51	1	a
5	6.65×10^{-7}	28.55	0.9981	a
6	2.43×10^{-5}	26.20	0.9995	a
7	3.65×10^{-6}	27.44	0.9999	a
8	3.48×10^{-6}	27.47	0.9999	a
9	2.10×10^{-6}	27.80	0.9996	a
(M_{res})-**10**	7.40×10^{-8}	29.98	0.9995	a
(P_{res})-**10**	2.96×10^{-7}	29.07	0.9997	a
11	8.15×10^{-5}	25.41	0.9997	a

[a] Method a: Off-column racemization experiments ($CHCl_3$, 55 °C, HPLC). Method b: ^{1}H NMR ([D_6]DMSO, 140 °C).

ment in the quality of the linear free-energy relationship (LFER) correlations. In other words, unfavorable LFERs obtained through descriptors calculated at low levels of theory do not afford definitive indication about their inadequacy, while, on the contrary, favorable findings are suggestive of their good sensitivity. Therefore, as a basic choice, also in view of the large number of molecular structures to model, we decided to assess the LFER descriptors by the fast AM1 semiempirical approach.

A preliminary evaluation of the capacity of each descriptor to monitor as a single probe of the variations in stereolability of selected compounds was limited to subensemble **SE_1** and compound **6** (see Supporting Information Table S2). Considering the expected difficulties that the use of a single descriptor entails in monitoring all electronic and structural factors responsible for the stereolability of such a variegated ensemble of phosphane oxides **1**–**11**, a more in-depth LFER investigation was carried out by resorting to multiparameter equations incorporating the most limited number of non-interrelated descriptors, chosen among those discussed above. The mathematical expression of such equations can be generalized as Equation (1)

$$\Delta G^{\neq}{}_{k} = \sum C_i D_i + C_0 \qquad (1)$$

where C_i and C_0 are coefficients evaluated by linear regression analysis, and the former modulate the effects monitored by the molecular descriptors D_i employed. Therefore, analyses based on type (1) equations were initially repeated on the subset of compounds **1**–**6** (Equations (1S)–(3S) in the Supporting Information). On the basis of the results obtained from these calculations (see Supporting Information), it was possible to give a preliminary rationalization of the experimental data.

Inspection of the data collected in Table 2 and Table S1 of the Supporting Information evidences that an increase in the $\Delta G^{\neq}$ barrier is observed when the positive atomic charge on the phosphorus atom is reduced and, conversely, when electron density on the P=O oxygen atom increases. A lower helix inversion barrier is found in correspondence with a reduction in $d_{P=O}$ values. A possible interpretation of these results is that the electronic effects produced by the substituents present on the blades, though modest, may affect the van der Waals volume of the phosphorus and oxygen atoms of the P=O group, and hence the hindrance that they may pose to blade rotation, by modulating their electron density and the length of the P=O bond. Thus, it seems logical to expect that a reduction in the van der Waals volume of the P atom (i.e., more positive δ_P values) might correspond to an increase in helix-inversion rate constant, while a growth of the O van der Waals volume (i.e., more negative δ_O values) corresponds to a slowdown of the process. It is also expected that the longer the P=O bond the higher the hindrance to blade rotation. In particular, it appears that $d_{P=O}$ is the most sensitive among the three molecular descriptors (see the relevant factor of statistical significance in Table S2 of the Supporting Information).

In conclusion, electron-withdrawing groups would decrease $\Delta G^{\neq}$ by reducing the electron density on both phosphorus and oxygen atoms of the P=O group, while the opposite should be expected from the action of electron-releasing substituents, as observed by comparing the data calculated for compounds **1**–**6** with those obtained for the reference compound **M0**, with the only, albeit macroscopic, exception of compound **3**, for which more marked stereolability would be expected (Figure 7, Table S1 and relevant comments in the Supporting Information).

According to the resonance structures **$RS3_{1-6}$** (Scheme 1), the electron-releasing effect of the ethoxyl group located in the 2-position of the naphthalene ring of all compounds **1**–**6** can be considered the main factor responsible for the calculated increase in P=O bond length relative to reference compound **M0**.

When, together with compounds **SE_1** and **6**, also the phosphane oxides belonging to subensemble **SE_2** were included in LFER analyses based on Equation (1S) (descriptors δ_P and δ_O), (2S) (descriptors δ_O and $d_{P=O}$) or (3S) (descriptors δ_P and $d_{P=O}$) of the Supporting Information, a dramatic reduction in r^2 was prevented only in the two last cases [r^2 was found to be 0.62 from Eq. (1S), 0.77 from Eq. (2S), and 0.71 from Eq. (3S)].

However, from the worst results derived from Equations (2S) and (3S) (see the SI), the $\Delta G^{\neq}$ values were reproduced with a maximum error of 0.6 kcal mol^{-1} and a standard error of only 0.38 kcal mol^{-1}. In contrast to what was found for the restricted set of compounds **1**–**6**, this result evidences the important role that the joint action of δ_P or δ_O with the descriptor $d_{P=O}$ may play in monitoring the stereolability of phosphane oxides like tris(1-naphthyl)phosphane oxide (**M0**) when the structure is made more complex through the insertion of a dioxene ring on the naphthalene moieties. In fact, by simple inspection of all the δ_P and δ_O values (Table S1 of Supporting Information), the large difference between subensembles **SE_1** and **SE_2** can be realized.

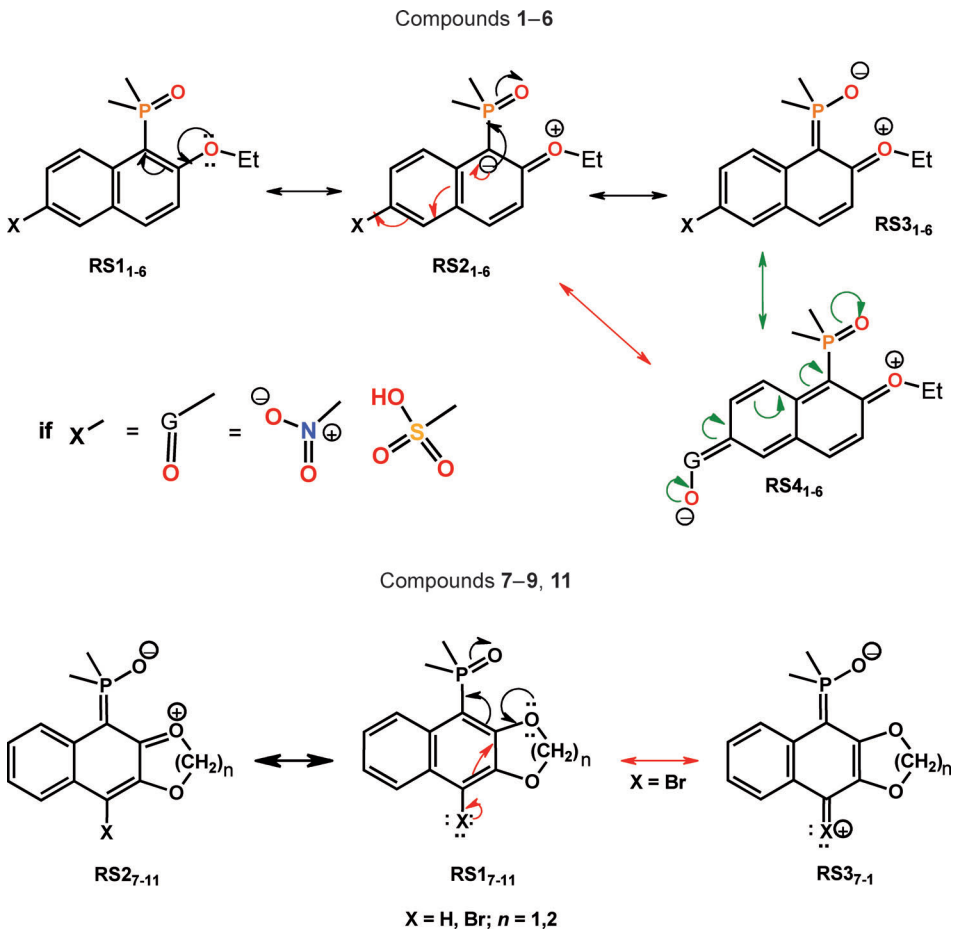

Scheme 1. Mesomeric effect involving the P=O group and the *ortho* oxygen atom of phosphane oxides **1**–**11**.

In comparison with compounds belonging to the **SE$_1$** group, the propellers of the **SE$_2$** group have phosphorus atoms with much less positive δ_P values, and oxygen atoms with much less negative δ_O values. These trends appear to be in opposition to each other in relation to the effect that they should produce on the enantiomerization barriers. Furthermore, the assessed $d_{P=O}$ values are always smaller. In the compounds belonging to subset **SE$_2$** the bromine atom shows an experimentally negligible effect on stereostability, according to the opposed inductive −I and mesomeric +M effects of the halogen atom (resonance structure **RS3$_{7-11}$** in Scheme 1). Such behavior seems to closely reflect the opposed changes observed for δ_P and δ_O.

Interestingly, when calculation of δ_P, δ_O, and $d_{P=O}$ was performed on the model tris[1-(2,3-dimethoxy)naphthyl]phosphane oxide (**M1**), obtained from **7** by breaking the C–C single bond of the dioxene ring of each blade, and tris[1-(2,3-diethoxy)naphthyl]phosphane oxide (**M2**), derived from **1** by ethoxylation of the 3-position of the naphthalene rings, the calculated values much more closely matched those characterizing phosphane oxides of the **SE$_1$** series (see Table S1 of the Supporting Information). This result confirms that the rigidity of the dioxene ring significantly affects the electronic (δ_P and δ_O) and structural ($d_{P=O}$) properties of the P=O group and influences the helix reversal barriers, which are different from those produced by the more conformationally mobile ethoxyl group of compounds **1**–**6** and model structures **M1** and **M2**.

A rough estimate of $\Delta G^{\neq}$ based on the multiparameter regression performed with Equation (3S) of the Supporting Information afforded for models **M1** and **M2** greater values than that calculated for compound **7** (+0.6 and +1.1 kcal mol^{-1}, respectively), in agreement with the higher experimental stability shown by **5** (the electronically most similar propeller to models **M1** and **M2**) with respect to **7**–**9**. These findings suggest that the dioxene ring is a structural component that slightly activates the helix inversion process, and justifies grouping compounds **7**–**9** in an individual subset (**SE$_2$**); hereafter, we designate the effect of the dioxene ring as $E_{dioxene}$.

We suggest that $E_{dioxene}$ may originate from the worse conjugation that the ring oxygen lone-pair can establish with the naphthalene ring. Conjugative electron donation would require trigonal sp^2 hybridization for the oxygen atom, a change that should lead to modest destabilization of the six-membered ring due to the increase in the C-O-C angle. To gain some indications on this point, we considered the O–C2 distance to the naphthalene ring (d_{C-O}, Table S1 of Supporting Information). Inspection of these data indicates that in compounds **7**–**9** the d_{C-O} value is greater, in accordance with a smaller contribution of resonance structure **RS2$_{7-11}$** compared to the corresponding **RS3$_{1-6}$** (Scheme 1). The increase in d_{C-O} for **7** is the greatest among those calculated for the whole series of compounds **1**–**9**. Concerning the modest electron-withdrawing action displayed by the nitro and sulfo substituents in compounds **2**–**4** and **6**, some relevant considerations are given in the Supporting Information.

Considering the tight structural analogies that phosphane oxides belonging to the **SE$_2$** subset share with compound **10**, it was logical to directly compare their experimental stereolabilities and the calculated electronic-effect descriptors. This could give information on the nature of the hindrance that double methyl substitution exerts on blade rotation. As expected, values of δ_P, δ_O, $d_{P=O}$, and d_{C-O} very close to those shown by **7** resulted, and thus suggest that methyl disubstitu-

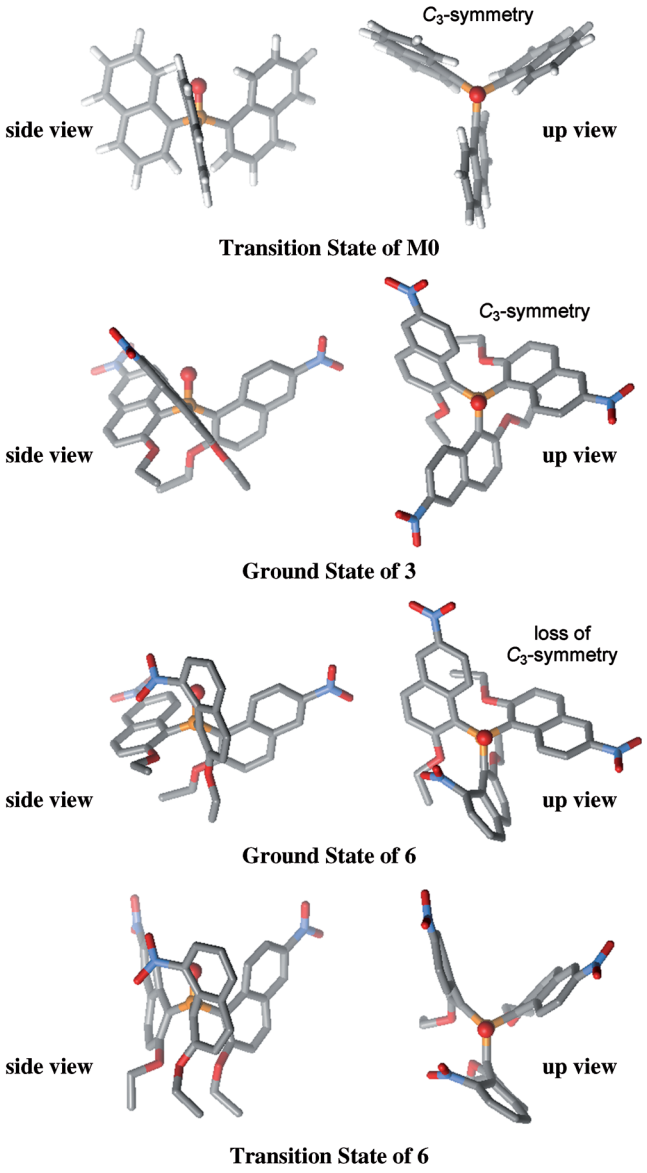

Figure 7. Calculated structures of ground and stationary states of compound **6** and of some other strictly related phosphane oxides.

tion in **10** has a negligible influence on the electronic and structural properties of the P=O framework. Classical steric interactions, leading to a strong increase in blade gearing, are evidently the main factor responsible for the $M_{res} \rightleftarrows P_{res}$ diastereomerization barrier of phosphane oxide **10**. In quantitative terms, from the difference among the $\Delta G^{\neq}$ values, it results that the insertion of the pair of equatorial methyl groups on the dioxene ring leads to a marked slowdown of the helix inversion process, corresponding to an increase in activation free energy of 1.63 kcal mol^{-1} for the (P_{res})-**10**→(M_{res})-**10** diastereomerization and 2.54 kcal mol^{-1} for the opposite (M_{res})-**10**→(P_{res})-**10** conversion. Surprisingly, the enantiomerization barrier of phosphane oxide **11**, which looks structurally more similar to compounds **7**–**10** than to **1**–**6**, was found to be the lowest.

A possible explanation for this observation could be suggested by considering the smaller size of the 1,3-dioxolene ring in comparison with the 1,4-dioxene system. The decrease of one carbon unit involves significant changes in the three-dimensional structure, both in terms of C-P-C angles and O-P-C1-C9 dihedral angles (see X-ray diffraction data above section and Table S1 of the Supporting Information). It is therefore expected that such remarkable differences might have an effect on the electronic properties of the P=O group. Comparative calculations for the couple **10**, **11** as well as for **11** and compounds **7**–**9** gave very different values for parameters δ_P, δ_O, $d_{P=O}$, and d_{C-O}. In particular, both the δ_P and δ_O descriptors determined for **11** suggested reduced electron density on the atoms constituting the P=O group, corresponding to increased stereolability. In addition, a smaller $d_{P=O}$ (the shortest one found in the whole series) and a greater d_{C-O} value point to a further loss in significance of the resonance structure **RS2**$_{7-11}$ in favor of **RS1**$_{7-11}$ (Scheme 1) and thus also to a contribution to a further drop in the enantiomerization barrier (i.e., a reduction in the $\Delta G^{\neq}$ similar to that defined above as $E_{dioxene}$ effect for compounds **7**–**9**, but of much greater importance, hereafter designated as $E_{dioxolene}$ effect). A further factor that could justify a less favorable conjugation between the lone pairs of the dioxolene oxygen atoms and the P=O bond is the O-P-C_1-C_9 torsion angle, which is about 42° in **11**, in contrast to the average value of 37° found for compounds **7**–**9**.

As the final test for the reliability of the theoretical approach, we propose two new regression analyses, based on Equations (4S) and (5S), which were derived from Equations (2S) and (3S) of the Supporting Information by inclusion of the $^{Ar}C-O^2$ bond length (d_{C-O}) as a further descriptor of the electronic effects. They were applied to the complete set of propellers **1**–**11**, with the sole exclusion of phosphane oxides **10**.

The LFER analysis based on Equation (4S) of the Supporting Information exhibited the best correlation (r^2= 0.909, see Figure 8 and the details reported in the Supporting Information), so that the parameters δ_O, $d_{P=O}$, and d_{C-O} can be proposed as a set of descriptors that are truly effective in monitoring the complex electronic contributions governing the helix inversion process of phosphane oxides **1**–**9** and **11**, regardless of the low level of theory used for their calculation. Finally, the observed inability of (M_{res})-**10** and (P_{res})-**10** to correlate according to Equations (4S) and (5S) of the Supporting Information is in agreement with the steric origin of their higher configurational stability, which arises from the insertion of two methyl groups on the dioxene ring and cannot be associated to electron-donating effects attributable to them.

In any case, before stating that there are only modest electronic influences on the configurational stability of tris-aryl phosphane oxides, we felt it necessary to quantitatively evaluate their electronic properties through experimental methods.

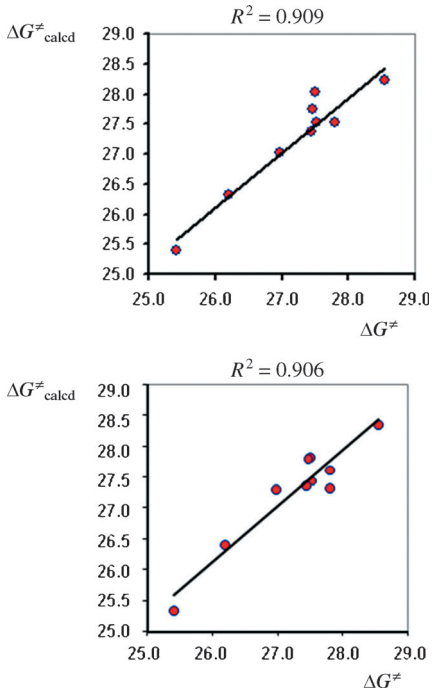

Figure 8. Free-energy linear relationships found for the set of phosphane oxides **1–9** and **11** by applying Equations (4S) and (6S) of the Supporting Information (top and bottom, respectively).

Experimental evaluation of the electronic properties of phosphane oxides: The electronic properties of phosphane oxides **1–11** were evaluated by cyclic voltammetry in acetonitrile solution, with inclusion in the study of the series of the corresponding blade bromides as reference (Figure 9). As a general rule, in a systematic series, under constant operating conditions, both the first oxidation and reduction peaks $E_{p,a}$ and $E_{p,c}$ should regularly shift in positive direction for increasingly electron poor systems (the easier the reduction, the more difficult the oxidation) and vice versa for increasingly electron rich systems. However, steric effects and different reaction mechanisms could significantly modulate the sequence, and therefore must also be taken into account.

Electrochemistry of blade bromides: Table 3 reports key CV data for the nine investigated blade bromides (for corresponding CV patterns, see Figure S10 in the Supporting Information). Comparison of the first reduction peaks provides the most convenient approach to the rationalization of the electronic properties of our substrate series, since blade bromide reduction corresponds to a well-defined process, resulting in bromine–carbon bond cleavage, and involves the same position to which the phosphorus atom is linked in the corresponding phosphane oxide series. Mechanistic details concerning specific blade bromides are provided in the Supporting Information. The first reduction peaks in the whole series can be satisfactorily rationalized in terms of Hammett parameters,[27] by considering the positions of the substituents on the naphthyl system with respect to the bromine reactive site:

1) The 2-positions (*ortho*) invariably carry an ethoxyl group (a methoxyl group in a single case), which should result in nearly constant inductive effects that can be considered a constant offset condition; therefore, no Hammett parameter has been assigned, and this is a convenient approach considering the unavailability of Hammett parameters for substituents located in *ortho* positions;
2) The substituent effects in the 3-positions (*meta*) are purely inductive and therefore were accounted for in terms of σ_m.

Table 3. First reduction peak potentials $E_{p,c}$ and first oxidation peak potentials $E_{p,a}$ of the blade bromides recorded on a GC electrode at 0.2 V s^{-1} in MeCN + 0.1 M TBAP with ohmic-drop compensation, in increasing order of reductive bromide cleavage capability. Sums of the relevant σ parameters are also reported.

Compound	Substituents	$\Sigma\sigma$	$E_{p,c}$ (onset)	$E_{p,c}$ (max)	κ	$E_{p,a}$ (onset)	$E_{p,a}$ (max)
11(b)	$OCH(CH_3)_2O$	0.10	−2.04	−2.28	0.50	1.42	1.71
7(b)	OCH_2CH_2O	0.12	−2.08	−2.23	0.58	1.33	1.64
10(b)	$OCH(CH_3)CH(CH_3)O$	0.10	−2.03	−2.20	0.68	1.32	1.55
5(b)	CH_3CH_2O, CH_3CH_2O	0.10	−2.00	−2.16	0.70	1.12	1.21
1(b)	CH_3CH_2O	0	−1.98	−2.11	0.70	1.39	1.52
1a(b)	CH_3O	0	−2.00	−2.17	0.67	1.38	1.52
8(b)	OCH_2CH_2O, Br	0.27	−1.81	−1.93	0.68	1.34	1.48
6(b′)	NO_2, CH_3CH_2O	0.71	−1.05	−1.12	0.84	1.66	1.77
3(b)	NO_2, CH_3CH_2O	0.71	−1.00	−1.11	0.71	1.66	1.81

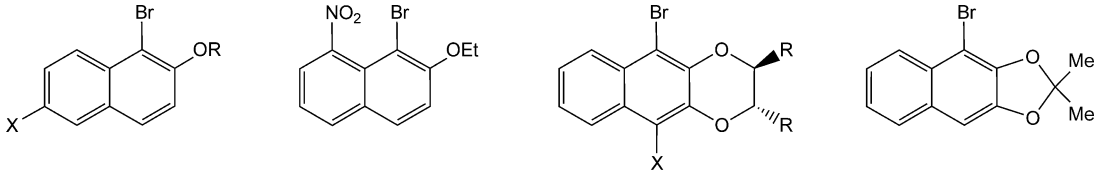

1a(b): R = Me, X = H

1(b): R = Et, X = H

3(b): R = Et, X = NO_2

5(b): R = Et, X = EtO

6(b)

7(b): X = R = H

8(b): X = Br, R = H

10(b): X = H, R = Me

11(b)

Figure 9. Blade bromides (i.e., the naphthalene derivatives displaying the same substitution pattern as the tris-naphthyl phosphane oxide blades, with a bromo substituent where the phosphorus atom is located).

3) The Br substituent effects in the 4-positions (*para*) involve mesomeric interactions and therefore were accounted for in terms of σ_p^+.
4) The effects of substituents located in the 6- and 8-positions were accounted for by σ_p parameters, taking into account that they occupy a dienyl-homologous position to the substituent in position *para* to the phosphorus atom, even though they do not directly interact with the reaction center.
5) The dioxene ring was considered as split into two methoxyl groups.
6) The dioxolene ring was considered as split into a methoxyl group in the 2-position and an isopropoxyl group in the 3-position.

Plotting cathodic peak and onset potentials versus the sum of the Hammett parameters $\Sigma\sigma$ resulting from the above criteria gives fairly linear correlations with significant slopes (Figure S11 in the Supporting Information).

The first oxidation peaks of the blade bromides, characterized by complex shapes and high currents, correspond to complex processes starting with formation of the radical cation and proceeding through several electron-transfer and chemical steps to give a variety of products, including dimers, trimers, electroactive oligomeric films, and quinoid species, depending on the reaction medium and on the nature and position of the alkoxyl substituents, whereby the *ortho*-dialkoxy case is an especially peculiar one.[28–30] For this reason an Hammett approach appeared hardly appropriate in the case of the blade bromide first oxidation peaks. In fact, they appear to be only slightly affected by substituent effects, with the exception of the strongly electron withdrawing nitro groups, which result in significant displacement towards more positive potentials, albeit less pronounced than in the case of reduction, when the electron transfer is localized on the nitro group.

In any case the oxidation process appears less appropriate for our aim of accounting for the electronic availability of the phosphorus atom in phosphanes, since, unlike bromide reduction, it does not involve the same position to which the phosphorus atom is linked in the corresponding phosphane oxide series.

Electrochemistry of phosphane oxides: A synopsis of the CV patterns of the twelve investigated phosphane oxides, ranked in decreasing order of oxidation facility, is provided in Figure 10. The corresponding $E_{p,a}$ and $E_{p,c}$ are collected in Table 4. Excluding **3**, **4**, and **6**, in which the first reduction peak involves the nitro groups, and **8** and **9**, in which it concerns the bromo groups, the first reduction peaks of the phosphane oxides are located at very negative potentials.

According to Savéant,[31] when working in an aprotic solvent with a quaternary ammonium salt as supporting electrolyte, the first reduction peaks of a tris-aryl phosphane or of a tris-aryl phosphane oxide should be related to a complex catalytic process with multiple competitive pathways, starting from formation of the phosphane oxide radical anion and involving partial alkylation of the phosphane oxide by reaction with the quaternary ammonium cation. This results in chemically reversible or partially reversible peaks at very negative potentials, near to the solvent background, which appears to hold for our phosphane oxide series for members having only alkoxyl substituents on the naphthyl blades.

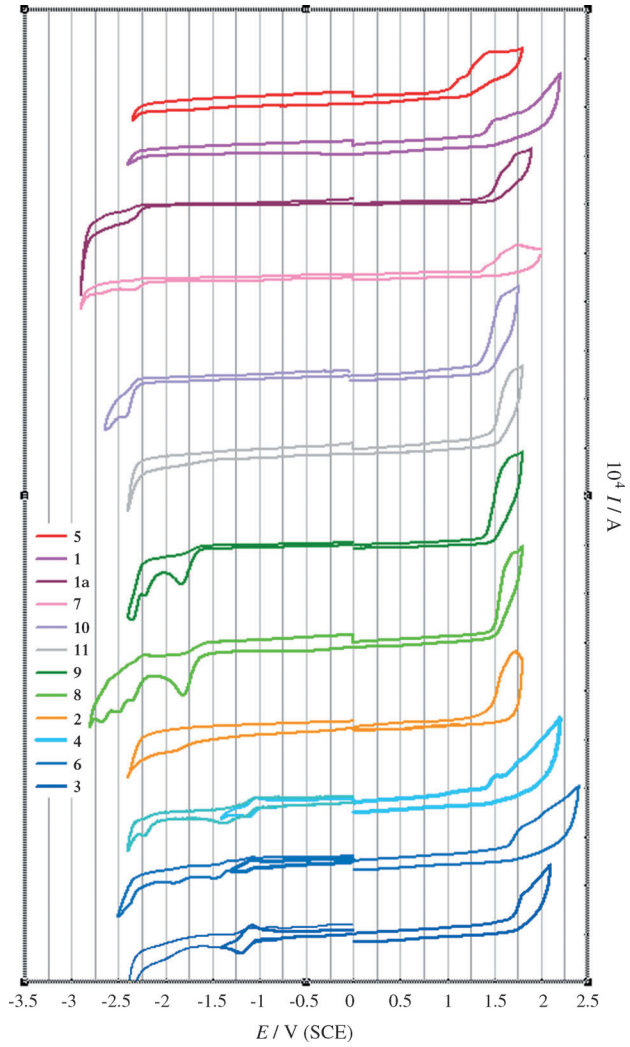

Figure 10. Synopsis of the CV patterns of the phosphane oxides recorded on GC electrode at 0.2 Vs^{-1} in MeCN + 0.1 M TBAP with ohmic-drop compensation.

The situation is different:

1) For substrates **8** and **9**, in which the first reduction peak concerns chemically irreversible two-electron reduction of the bromo groups producing the corresponding dehalogenated aryl systems, as previously discussed in the case of the bromo-substituted blade series. However, sequences of two or three reversible reduction peaks were observed at potentials more negative than the first one, which could be associated with subsequent reduction of the dehalogenated phosphane oxide by the Savéant catalytic mechanism discussed in the Supporting Information

Table 4. First reduction peak potentials $E_{p,c}$, and first oxidation potential onsets $E_{p,a\ (onset)}$, and maxima $E_{p,a\ (max)}$ of the phosphane oxides, at 0.2 V s^{-1}, in MeCN + 0.1 M TBAP, with ohmic-drop compensation, in increasing order of oxidation facility. Sums of the relevant σ parameters are also reported.

Compound	Substituents	σ_{max}	$E_{p,c}$ (onset)	$E_{p,c}$ (max)	σ_{min}	$E_{p,a}$ (onset)	$E_{p,a}$ (max)
5	2 EtO	0.10	n.d	n.d	0.10	0.96	1.13, 1.48
1	EtO	0	n.d	n.d	0	1.35	1.52, 1.70
1a	MeO	0	−2.22	−2.42	0	1.41	1.53
7	OCH_2CH_2O	0.12	−2.23	−2.36	0.12	1.37	1.64
10	OCHMeCHMeO	0.10	−2.27	−2.38, −2.58 (diast. I) −2.38, −2.57 (diast. II)	0.10	1.40 1.38	1.60 1.62
11	$OCMe_2O$	0.10	−2.24	n.d.	0.10	1.49	1.70
9	OCH_2CH_2O (×1); OCH_2CH_2O, Br (×2)	0.27	−1.66	−1.86, −2.23, −2.35	0.12	1.39	1.68
8	OCH_2CH_2O, Br	0.27	−1.61	−1.81, −2.35, −2.50, −2.68	0.27	1.47	1.62, 1.70
2	SO_3H, EtO	0.30	−1.72	−1.9	0.30	1.38	1.60, 1.72
4	EtO (×2); NO_2, EtO (×1)	0.71	−1.00	−1.15,[a] −1.40, −2.21	0	1.34	1.52
6	NO_2, EtO (×2); NO_2('), EtO (×1)	0.71	−1.03	−1.18,[b] −1.46, −1.91, −2.37	0.71	1.65	1.81
3	NO_2, EtO	0.71	−1.01	−1.19,[c] −2.02	0.71	1.68	1.82

[a] $E_p - E_{p/2} = 0.065$ V. [b] $E_p - E_{p/2} = 0.065$ V. [c] $E_p - E_{p/2} = 0.080$ V.

(or, more simply, to subsequent reduction of each blade to the corresponding stable radical anion).

2) For substrates **3**, **4**, and **6**, featuring nitro substituents on the blades, for which the first reduction peak concerns the electrochemically and chemically reversible monoelectronic reduction to stable nitro radical anions. In the case of C_3-symmetric **3** it is particularly interesting that the three nitro redox centers give a single reversible peak corresponding to three electrons, as expected, but of 0.080 V half-peak width, that is much larger than the value of 0.057 V expected for a reversible one-electron transfer, or for three fully equivalent and independent monoelectronic redox centers. This could point to some significant interaction in the space between the three nitro groups, so that radical anion formation on one of them partially hinders the same process on the other two, and slightly different potentials result.

In any case, a fairly linear Hammett relationship was observed for reduction peak potentials in the phosphane oxides series, too, with an even better slope than in the bromide blade case (Figure 11).

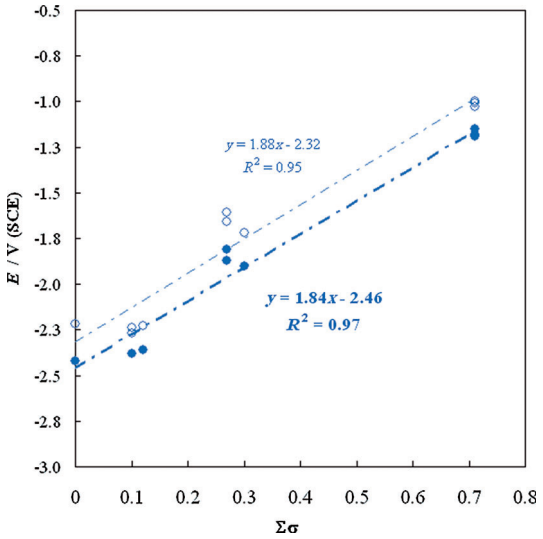

Figure 11. Hammett relationships concerning the first reduction peak potentials (onset: empty circles, peak: full symbols) for the phosphane oxide series.

The first oxidation should occur on the blades and with the same complex reaction pathways mentioned above in the case of the bromide blades, highly dependent on steric parameters. Therefore, the Hammett approach is not as appropriate as in the reduction case, and the only substituent resulting in significant electronic effects is the nitro group. This can be perceived even within the same molecule, in the case of unsymmetrical phosphane oxide **4**, having a first oxidation peak at 1.34 V, corresponding to the electron richer blades decorated with alkoxyl groups, and a subsequent oxidation peak at 1.52 V, corresponding to the electron poorer blade featuring the nitro substituent. In the case of **10**, for which two diastereoisomers are available, a slight difference seems to be perceptible, as expected, particularly in the oxidative CV pattern.

As in the blade bromide series, clues to the effect of the steric hindrance of cyclic diethers could be deduced from the degree of electronic availability of the blades expressed through the experimental oxidation potentials. In particular, the presence of a cyclic diether group condensed with the naphthalene ring leads to an increase in $E_{p,a}$ (i.e., to an increase in electron-deficient character) in phosphane oxides **7**, **10**, and **11** (cf. $E_{p,a}$ values of **7**, **10**, and **11** with those of **1** and **1a**). This observation is in agreement with the above defined $E_{dioxene}$ and $E_{dioxolene}$ effects, which were attributed to loss of conjugation between the lone pairs of the dioxene or dioxolene oxygen atoms and the P=O bond, which is expected to be more pronounced for the five-membered ring of **11**. Coherent with these findings, a correlation of quality equivalent to that found by using Equation (4S) of the Supporting Information was obtained when the descriptor d_{C-O} was substituted with the $E_{p,a}$ values in the Equation (6S) of the Supporting Information ($r^2 = 0.906$, Figure 8 and Table S1 of Supporting Information). We conclude that a good relationship exists between the experimental electronic availability of the phosphane oxides, expressed through oxi-

dation potentials, and the calculated conjugation extent between the naphthalene ring and the lone pair of the oxygen atom in the 2-position.

Conclusion

We have shown that the helix inversion barrier controlling the configurational stability of tris-aryl phosphane oxides existing as stable residual stereoisomers is only moderately dependent on the electronic availability of the substrate, while steric factors play the dominant role in the M_0 stereoisomerization process. This conclusion is founded on the results of a series of multidisciplinary experiments based on the following research plan:

1) A series of eleven differently substituted tris-aryl phosphane oxides was synthesized and all members fully structurally characterized.
2) All of the residual racemates, except for **2**, were resolved into antipodes by semipreparative HPLC on a polysaccharide-based chiral stationary phase, while the residual diastereoisomers of **10** could also be separated by chromatography on a silica-gel column.
3) The chiroptical properties of all residual stereoisomers were determined and the absolute configuration descriptors M_{res} or P_{res} assigned to them, either directly by single-crystal anomalous X-ray diffraction analysis or by correlation of the CD spectra.
4) The energy barriers for activation of the M_0 mechanism, which is responsible for the instability of the residual stereoisomers, were evaluated for all compounds by stereoisomerization kinetics studies on the stereomerically pure compounds, or by ^{1}H and ^{31}P NMR techniques. All residual stereoisomers were found to be configurationally quite stable compounds with racemization activation energies between 25 and 29 kcal mol^{-1}.
5) Cyclovoltammetry was performed to quantitatively evaluate the electronic properties of the phosphane oxides in terms of their reduction and oxidation peak potentials and, as a simpler model, those of the corresponding single blades having a bromine substituent where the phosphorus atom is located. The results were satisfactorily rationalized in terms of Hammett parameters; moreover, they confirmed that, as pointed out by theoretical computations, cyclic diether substituents lower the electron availability of the aromatic blades with respect to a single alkoxyl group.
6) Compounds displaying very different electronic properties and very similar steric properties were found to have very similar configurational stability ($\approx$27 kcal mol^{-1}), while the most sterically encumbered M_{res} and P_{res} residual diastereoisomers **10** were found to have the highest configurational stability (28–30 kcal mol^{-1}).
7) Theoretical analysis furnished a quite clear, rational, and persuasive picture of the possible way in which electronic effects may modulate the stereolability of the investigated phosphane oxides and gave evidence, in particular, on the crucial role played by the presence of constrained cyclic diether moieties condensed with the naphthalene blades.

The natural next step is extension of this work to check possible access to configurationally stable residual monodentate tris-aryl phosphane ligands for transition metals in homogeneous stereoselective catalysis.

Experimental Section

Organic synthesis: Melting points were measured with Büchi B-540 instruments. NMR spectra were recorded on Bruker AV 400 and Bruker AC 300 spectrometers. Chemical shifts are given in parts per million (ppm) and the coupling constants in hertz. Mass spectra were recorded on Bruker Daltonics high-resolution FT-ICR model APEXTM II (4.7 T Magnex cryomagnet with ESI source) and Thermo Finnigan LCQ Advance (APCI). Purification by column chromatography was performed by using Merck silica gel 60 (230–400 mesh for flash-chromatography and 70–230 mesh for gravimetric chromatography).

Synthesis of phosphane oxides: Compounds **1** and **7** were previously described by us.[6] Phosphane oxides **1a**, **2**, **5**, **10**, and **11** were prepared by hydrogen peroxide oxidation of the corresponding phosphanes.[9] Aqueous H_2O_2 solution (2–3 drops of a 33% solution in 1–2 mL of water) was added to a solution of the phosphane (about 50 mg) in CH_2Cl_2 (5 mL) and the reaction mixture was vigorously stirred overnight at room temperature. The organic layer was separated, washed with water, dried (Na_2SO_4), and concentrated under reduced pressure to give the crude phosphane oxide, which was purified according to the procedures described below.

Tris[1-(2-methoxy)naphthyl]phosphane oxide (1a): Crude phosphane oxide was purified by chromatography on a silica-gel column (CH_2Cl_2/AcOEt 9/1) to give **1a** as a colorless solid (yield 80%). M.p. 274–277 °C (sint. 263 °C); ^{1}H NMR (300 MHz, $CDCl_3$): δ = 9.01–8.97 (m, 3H), 7.88 (d, ^3J(H,H) = 8.98 Hz, 3H), 7.80–7.70 (m, 3H), 7.36–7.29 (m, 6H), 7.08 (dd, ^3J(H,H) = 9.07 Hz, ^4J(H,P) = 5.19 Hz, 3H), 2.87 ppm (s, 9H); APT NMR (400 MHz, $CDCl_3$): δ = 158.32 (d, ^2J(C,P) = 2.72 Hz), 135.39 (d, ^2J(C,P) = 6.64 Hz), 133.29 (d, ^4J(C,P) = 1.81 Hz), 129.83 (d, ^3J(C,P) = 9.76 Hz), 128.02 (s), 127.18 (d, ^3J(C,P) = 5.53 Hz), 126. 96 (s), 123.87 (s), 119.78 (d, ^1J(C,P) = 109.08 Hz), 114.42 (d, ^3J(C,P) = 7.75 Hz), 56.36 ppm (s); ^{31}P NMR (300 MHz, $CDCl_3$): δ = 20.88 ppm (s); MS (APCI): m/z: 518.5 $[M]^+$.

Tris[1-(2-ethoxy-6-sulfonato)naphthyl]phosphane oxide (2): Crude phosphane oxide was triturated with acetone to give **2** as a pale yellow solid (yield 80%). M.p. 199–201 °C; ^{1}H NMR (300 MHz, CD_3OD): δ = 8.38 (br s, 3H), 8.28 (d, ^3J(H,H) = 9.16 Hz, 3H), 8.27 (d, ^3J(H,H) = 9.31 Hz, 3H), 7.67 (dd, ^3J(H,H) = 9.16 Hz, ^4J(H,H) = 1.70 Hz, 3H), 7.42 (dd, ^3J(H,H) = 9.31 Hz, ^4J(H,P) = 5.99 Hz, 3H), 3.95–3.82 (m,3H), 3.64–3.51 (m, 3H), 0.43 ppm (t, ^3J(H,H) = 6.99 Hz, 9H); ^{31}P NMR (300 MHz, MeOD): δ = 33.38 ppm (s); APT NMR (300 MHz; CD_3OD): δ = 162.39 (s), 141.35 (s), 137.89 (s), 136.64 (d, ^2J(C,P) = 6.04 Hz), 129.72 (d, ^3J(C,P) = 9.81 Hz), 127.67 (s), 126.61 (d, ^3J(C,P) = 6.04 Hz), 125.37 (s), 115.92 (d, ^3J(C,P) = 7.55 Hz), 114.11 (d, ^1J(C,P) = 114.71 Hz), 65.71 (s), 13.80 ppm (s); MS (ESI): m/z (%): 799.2 (100) $[M+H]^+$.

Tris[1-(2,6-diethoxy)naphthyl]phosphane oxide (5): Crude phosphane oxide was purified by chromatography (silica gel, CH_2Cl_2/AcOEt 9/1) to give **5** as a white solid (yield 72%). M.p. 264.8–266.9 °C; ^{1}H NMR (300 MHz, $CDCl_3$): δ = 8.88 (d, ^3J(H,H) = 9.30 Hz, 3H), 7.73 (d, ^3J(H,H) = 9.30 Hz, 3H), 7.05 (br s, 3H), 7.00–6.92 (m, 6H), 4.09 (q, ^3J(H,H) = 6.90 Hz, 6H), 3.72–360 (m, 3H), 3.32–3.208 (m, 3H), 1.42 (t, ^3J(H,H) = 6.90 Hz, 9H), 0.37 ppm (t, ^3J(H,H) = 6.90 Hz, 9H); ^{13}C NMR (300 MHz, $CDCl_3$): δ = 156.46 (s), 154.91 (s), 131.91 (s), 131.08 (d, ^2J(C,P) = 6.64 Hz), 130.66 (d, ^2J(C,P) = 9.51 Hz), 128.84 (d, ^3J(C,P) =

5.21 Hz), 119.25 (d, ^1J(C,P) = 108.60 Hz), 119.09 (s), 114.41 (d, ^4J(C,P) = 7.40 Hz), 107.33 (s), 64.10 (s), 63.25 (s), 14.82 (s), 13.49 ppm (s); ^{31}P NMR (300 MHz, $CDCl_3$): δ = 21.97 ppm (s); MS (ESI): *m/z* (%): 693.4 (17) $[M+H]^+$, 715.4 (80) $[M^+ + Na]$, 242 (100); MS (EI^+): *m/z* (%): 692 (21) $[M^+]$, 647 (6), 243 (100), 216 (19).

Tris(5-{(2*S*,3*S*)-2,3-dihydro-2,3-dimethylnaphtho[2,3-*b*]-1,4-dioxinyl})-phosphane oxide (10): The mixture of the two diastereomeric phosphane oxides [yield 98%, MS (EI^+): *m/z* (%): 686 (46) $[M^+]$, 473 (93), 457 (72), 401 (51), 214 (79), 244 (77), 298 (75), 91 (100%)] was separated by chromatography on a silica-gel column (CH_2Cl_2/AcOEt 10/0.5).

First-eluted (M_{res}) diastereoisomer: R_f = 0.4 in CH_2Cl_2/AcOEt (10/0.5), pale yellow solid (yield of isolated compound 22%). M.p. 318–320 °C; ^{1}H NMR (300 MHz, $CDCl_3$): δ = 8.75 (d, ^3J(H,H) = 8.6 Hz, 3H), 7.64 (d, ^3J(H,H) = 8.1 Hz, 3H), 7.32 (s, 3H), 7.29–7.25 (m, 3H), 7.20–7.16 (m, 3H), 3.73 (quintet, ^3J(H,H) = 6.4 Hz, 3H), 2.78 (quintet, ^3J(H,H) = 6.4 Hz, 3H), 1.07 (d, ^3J(H,H) = 6.3 Hz, 9H), 0.36 ppm (d, ^3J(H,H) = 6.3 Hz, 9H,); APT NMR (300 MHz, $CDCl_3$): δ = 145.61 (d, ^2J(C,P) = 3.85 Hz), 142.76 (d, ^3J(C,P) = 10.72 Hz), 130.59 (d, ^2J(C,P) = 5.89 Hz), 130.19 (d, ^3J(C,P) = 11.02 Hz), 126.92 (d, ^3J(C,P) = 5.58 Hz), 126.83 (s), 124.69 (s), 124.29 (s), 118.18 (d, ^1J(C,P) = 107.24 Hz), 115.47 (s), 74.22 (s), 73.66 (s), 16.95 (s), 15.64 ppm (s); ^{31}P NMR (300 MHz, $CDCl_3$): δ = 17.19 ppm (s).

Second-eluted (P_{res}) diastereoisomer: R_f = 0.25 in CH_2Cl_2/AcOEt (10/0.5), yellow solid (yield of isolated compound 13%). M.p. 318.5–320.0 °C; ^{1}H NMR (300 MHz, $CDCl_3$): δ = 8.84 (d, ^3J(H,H) = 8.7 Hz, 3H), 7.61 (d, ^3J(H,H) = 8.1 Hz, 3H), 7.33 (s, 3H), 7.28–7.14(m, 6H), 3.58 (quintet, ^3J-(H,H) = 6.8 Hz, 3H), 3.28 (quintet, ^3J(H,H) = 6.5 Hz, 3H), 1.14 (d, ^3J-(H,H) = 6.4 Hz, 9H), 0.17 ppm (d, ^3J(H,H) = 6.4 Hz, 9H); APT NMR (300 MHz, $CDCl_3$): δ = 145.81 (d, ^2J(C,P) = 3.70 Hz), 142.64 (d, ^3J(C,P) = 10.72 Hz), 131.49 (d, ^2J(C,P) = 5.96 Hz), 129.64 (d, ^3J(C,P) = 11.32 Hz), 126.86 (d, ^3J(C,P) = 5.66 Hz), 126.76 (s), 124.64 (s), 123.93 (s), 117.73 (d, ^1J(C,P) = 106.64 Hz), 115.93 (s), 74.99 (s), 73.38 (s), 16.81 (s), 15.30 ppm (s); ^{31}P NMR (300 MHz, $CDCl_3$): δ = 17.98 ppm (s).

Tris[4-(2,2-dimethylnaphtho[2,3-*d*]-1,3-dioxolyl)]phosphane oxide (11): The crude phosphane oxide was treated with CH_2Cl_2 to give **11** as a colorless solid (yield 86%). M.p. 351–353 °C; ^{1}H NMR (300 MHz, $CDCl_3$): δ = 9.10–9.00 (m, 3H), 7.64–7.55 (m, 3H), 7.35–7.23 (m, 6H), 7.09 (s, 3H), 1.29 (s, 9H), 0.59 ppm (s, 9H); APT NMR (300 MHz, $CDCl_3$): δ = 150.03 (d, ^2J(C,P) = 4.07 Hz), 146.85 (d, ^3J(C,P) = 11.02 Hz), 132.02 (d, ^2J-(C,P) = 5.89 Hz), 130.56 (d, ^3J(C,P) = 9.28 Hz), 127.03 (s), 126.52 (d, ^3J-(C,P) = 5.36 Hz), 125.12 (s), 124.38 (s), 117.25 (s), 107.73 (d, ^1J(C,P) = 110.03 Hz), 107.21 (s), 25.50 (s), 24.17 ppm (s); ^{31}P NMR (300 MHz, $CDCl_3$): δ = 13.11 ppm (s); MS (ESI^+): *m/z* (%): 667.5 (100) $[M+Na]^+$, 645.5 (54) $[M+H]^+$.

Tris[1-(2-ethoxy-6-nitro)naphthyl]phosphane oxide (3) and bis[1-(2-ethoxy-6-nitro)naphthyl][1-(2-ethoxy-8-nitro)naphthyl]phosphane oxide (6): Nitric acid (65% 8.0 mmol, 0.79 mL) was dropped into a solution of tris[1-(2-ethoxy)naphthyl]phosphane[6] (1.09 g, 2.0 mmol) in $CHCl_3$ (10 mL) with vigorous stirring under nitrogen. The reaction mixture was warmed to 50 °C, after 6 h a second addition of nitric acid (12 mmol, 1 mL) was made, and then the reaction mixture was stirred overnight. The precipitated solid was collected by filtration and the organic layer was washed with water (10 mL), dried, and the solvent evaporated under reduced pressure to give a residue, which was purified by chromatography on a silica-gel column (CH_2Cl_2/AcOEt 10/0.5). Compound **3** was eluted first (300 mg, yield 22%). M.p. 303–304 °C; ^{1}H NMR (300 MHz, $CDCl_3$): δ = 9.05 (d, ^3J(H,H) = 9.66 Hz, 3H), 8.74 (brs, 3H), 8.13 (d, ^3J-(H,H) = 9.27 Hz, 3H), 8.04 (dd, ^3J(H,H) = 9.65 Hz, ^4J(H,H) = 2.46 Hz, 3H), 7.23 (dd, ^3J(H,H) = 9.30 Hz, ^4J(H,P) = 5.10 Hz, 3H), 3.86–3.74 (m, 3H), 3.55–3.44 ppm (m, 3H), 0.43 (t, J = 7.05 Hz, 3H); ^{31}P NMR (300 MHz, $CDCl_3$): δ = 20.33 ppm (s); APT NMR (300 MHz; $CDCl_3$): δ = 160.95 (s), 144.05 (s), 139.37 (d, ^2J(C,P) = 6.79 Hz), 136.50 (s), 128.53 (d, ^3J(C,P) = 4.90 Hz), 128.28 (d, ^3J(C,P) = 9.43 Hz), 125.38 (s), 120.93 (s), 118.67 (d, ^1J(C,P) = 109.13 Hz), 115.43 (d, ^3J(C,P) = 8.23 Hz), 64.64 (s), 13.83 ppm (s); MS (EI^+): *m/z* (%): 695 (2) $[M]^+$, 666 (7), 650 (27), 463 (52), 244 (100). The following fractions contained **6** (570 mg, yield 43%). M.p. 301–303 °C; ^{1}H NMR (300 MHz, $CDCl_3$; all signals in the spectrum recorded at room temperature are broad and unresolved): δ = 8.78–8.60 (brm, 2H), 8.55 (brs, 1H), 8.31 (brd, ^3J(H,H) = 7.50 Hz, 1H), 8.14 (brd, ^3J(H,H) = 8.70 Hz, 1H), 8.08–7.83 (brm, 5H), 7.56–7.38 (brm, 3H), 7.18–7.07 (brm, 1H), 7.05–6.94 (brm, 1H), 4.35–4.19 (brm, 1H), 4.09–3.94 (brm, 1H), 3.93–3.66 (brm, 2H), 3.64–3.49 (brm, 1H), 3.32–3.13 (brm, 1H), 0.91 (brt, J = 6.00 Hz, 3H), 0.63 (brt, J = 6.00 Hz, 3H), 0.27 ppm (brt, J = 6.00 Hz, 3H). The signals progressively sharpen with increasing temperature in [D_6]DMSO. ^{1}H NMR (300 MHz, DMSO, 400 K): δ = 8.86 (brt, 1H), 8.71 (brt, 1H), 8.57 (d, ^3J(H,H) = 9.54 Hz, 1H), 8.40 (d, ^3J-(H,H) = 9.17 Hz, 1H), 8.30 (d, ^3J(H,H) = 9.04 Hz, 1H), 8.27 (d, ^3J(H,H) = 8.88 Hz, 1H), 8.24 (d, ^3J(H,H) = 7.58 Hz, 1H), 8.15 (d, ^3J(H,H) = 9.09 Hz, 1H), 8.04 (d, ^3J(H,H) = 9.67 Hz, 1H), 7.83 (dd, ^3J(H,H) = 9.57 Hz, ^4J-(H,H) = 2.51 Hz, 1H), 7.66 (dd, ^3J(H,H) = 9.21 Hz, ^4J(H,H) = 5.35 Hz, 1H), 7.58 (t, ^3J(H,H) = 7.80 Hz, 1H), 7.48–7.37 (m, 2H), 7.28 (dd, ^3J-(H,H) = 9.11 Hz, ^4J(H,P) = 4.79 Hz, 1H), 4.30–4.16 (m, 1H), 4.14–3.96 (m, 1H), 3.96–3.76 (m, 2H), 3.71–3.57 (m, 1H), 3.50–3.37 (m, 1H), 0.86 (t, ^3J(H,H) = 6.98 Hz, 3H), 0.70 (t, ^3J(H,H) = 6.96 Hz, 3H), 0.39 ppm (t, ^3J(H,H) = 7.00 Hz, 3H); APT NMR (300 MHz; DMSO): δ = 161.33 (s), 161.12 (s), 147.20 (s), 142.58 (s), 142.00 (s), 138.89 (d, ^2J(C,P) = 5.96 Hz), 137.04 (d, ^2J(C,P) = 6.57 Hz), 136.34 (s), 135.48 (s), 135.12 (s), 134.63 (s), 130.01 (d, ^3J(C,P) = 9.36 Hz), 127.37 (d, ^3J(C,P) = 9.43 Hz), 127.18 (d, ^3J-(C,P) = 10.04 Hz), 126.84 (s), 126.34 (d, ^2J(C,P) = 4.00 Hz), 125.98 (s), 125.19 (s), 125.13 (s), 122.26 (s), 119.09 (s), 118.23 (s), 118.08 (d, ^1J-(C,P) = 107.32 Hz), 117.89 (d, ^1J(C,P) = 113.88 Hz), 117.13 (d, ^1J(C,P) = 112.98 Hz), 116.87 (d, ^4J(C,P) = 6.79 Hz), 115.22 (d, ^3J(C,P) = 6.11 Hz), 114.58 (d, ^3J(C,P) = 6.64 Hz), 64.86 (s), 63.57 (s), 63.47 (s), 13.53 (s), 13.16 (s), 12.64 ppm (s); ^{31}P NMR (300 MHz, $CDCl_3$): δ = 19.68 ppm (s); ^{31}P NMR (300 MHz, DMSO): δ = 20.10 ppm (s); MS (EI): *m/z* (%): 695 (4) $[M]^+$, 649 (100), 604 (11), 575 (17), 449 (28), 189 (29); UV ($c = 1.77 \times 10^{-5}$ in $CHCl_3$): λ_{max} (ε) = 244 (31192), 287 (23932), 347 (13672).

Bis[1-(2-ethoxy)naphthyl][1-(2-ethoxy-6-nitro)naphthyl]phosphane oxide (4): Nitric acid (65%, 1.4 mmol, 0.28 mL) was dropped into a solution of tris[1-(2-ethoxynaphthyl)]phosphane[6] (0.52 g, 1.0 mmol) in $CHCl_3$ (25 mL) with vigorous stirring under nitrogen at 35 °C. The reaction mixture was stirred for 3.5 h and then treated with cold 10% K_2CO_3 solution. The organic layer was dried over Na_2SO_4 and the solvent evaporated under reduced pressure to give a residue, which was purified by chromatography on a silica-gel column (CH_2Cl_2/AcOEt 10/0.3). The main fractions eluted contained compound **4** (114 mg, yield 19%): M.p. 272–273; ^{1}H NMR (300 MHz, $CDCl_3$): δ = 9.29 (d, ^3J(H,H) = 9.66 Hz, 1H), 8.93 (d, ^3J(H,H) = 8.28 Hz, 1H), 8.87 (d, ^3J(H,H) = 8.37 Hz, 1H), 8.74 (brs, 1H), 8.09 (d, ^3J(H,H) = 9.14 Hz, 1H), 8.04 (dd, ^3J(H,H) = 9.65 Hz, ^4J(H,H) = 2.51 Hz, 1H), 7.94 (d, ^3J(H,H) = 9.09 Hz, 2H), 7.84–7.76 (brm, 2H), 7.39–7.25 (brm,4H), 7.22 (dd, ^3J(H,H) = 9.15 Hz, ^4J(H,P) = 4.91 Hz, 1H), 7.09 (dd, ^3J(H,H) = 9.03 Hz, ^4J(H,P) = 5.35 Hz, 2H), 3.89–3.68 (m, 3H), 3.54–3.39 (m, 2H), 3.39–3.26 (m, 1H), 0.48 (t, ^3J(H,H) = 7.02 Hz, 3H), 0.45 (t, ^3J(H,H) = 7.02 Hz, 3H), 0.38 (t, ^3J(H,H) = 7.01 Hz, 3H); ^{31}P NMR (300 MHz, $CDCl_3$): δ = 21.35 ppm (s); APT NMR (300 MHz; $CDCl_3$): δ = 160.68 (s), 158.05 (s), 157.71 (s), 142.54 (s), 139.29 (d, ^2J(C,P) = 7.02 Hz), 135.80 (d, ^2J(C,P) = 6.87 Hz), 135.71 (d, ^2J(C,P) = 7.09 Hz), 135.14 (s), 133.85 (s), 129.44 (d, ^3J(C,P) = 10.11 Hz), 128.81 (d, ^3J(C,P) = 5.06 Hz), 128.26 (s), 128.23 (s), 127.67 (d, ^3J(C,P) = 8.60 Hz), 126.99 (s), 126.86 (d, ^3J(C,P) = 11.02 Hz), 126.78 (d, ^3J(C,P) = 11.02 Hz), 124.72 (s), 123.72 (s), 123.60 (s), 119.88 (s), 119.10 (d, ^1J(C,P) = 42.72 Hz), 118.82 (d, ^1J(C,P) = 75.32 Hz), 115.17 (d, ^3J(C,P) = 7.32 Hz), 113.47 (d, ^3J(C,P) = 8.08 Hz), 64.07 (s), 63.95 (s), 63.86 (s), 13.56 (s), 13.33 (s), 13.25 ppm (s). MS (EI): *m/z* (%): 605 (12.5) $[M]^+$, 576 (10), 560 (49), 418 (54), 373 (31), 361 (33), 199 (100), 172 (34). If the reaction mixture was stirred for 17 h, the final yield of the mono-nitro derivative **4** decreased while that of trinitro compound **3** increased to 62%.

Tris(5-{10-bromo-2,3-dihydronaphtho[2,3-*b*]-1,4-dioxinyl}phosphane oxide (8): Freshly crystallized NBS (268 mg, 1.5 mmol) was added to a solution of tris(5-[2,3-dihydronaphtho[2,3-*b*]-1,4-dioxinyl]phosphane oxide (**7**, 293 mg, 0.49 mmol) in 50% $CHCl_3$/AcOH (40 mL). The reaction mixture was stirred at room temperature for 4 d, water (3 × 40 mL) was added, the organic layer separated, washed with saturated solution K_2CO_3 (3 × 40 mL), and dried (Na_2SO_4), and the solvent removed under reduced pressure to give a residue, which was purified by chromatography on a silica-gel column (CH_2Cl_2/AcOEt 9/1). Compound **8** (403 mg, yield 98%) was obtained in pure state as a white solid (403 mg, yield

98%). M.p. 335–338°C (sint. 328–330°C); ^{1}H NMR (300 MHz, $CDCl_3$): δ=8.99 (d, ^3J(H,H)=8.52 Hz, 3H), 8.21 (d, ^3J(H,H)=8.45 Hz, 3H), 7.48–7.42 (m, 3H), 7.33–7.26 (m, 3H), 4.28–4.20 (m, 3H), 4.13–4.06 (m, 3H), 3.59–3.52 (m, 3H), 3.18–3.11 ppm (m, 3H); ^{31}P NMR (300 MHz, $CDCl_3$): δ=19.09 ppm (s); APT NMR (300 MHz; $CDCl_3$): δ=145.08 (d, ^2J(C,P)=4.23 Hz), 140.16 (d, ^3J(C,P)=11.09 Hz), 130.48 (d, ^2J(C,P)=6.64 Hz), 128.63 (d, ^3J(C,P)=11.24 Hz), 126.61–126.29 (d overlap with s), 125.87 (s), 125.82 (s), 117.78 (d, ^1J(C,P)=108.90 Hz), 112.48 (d, ^2J(C,P)=3.40 Hz), 64.46 (s), 63.15 ppm (s); MS (ESI): *m/z* (%): 837.0 (40.2), 839.0 (94.1), 841.0 (100), 843.0 (41.6) [M^++1]; 532.4 (90.9), 533.4 (34.6); MS (EI$^+$): *m/z* (%): 836 (10.5), 838 (35.2), 840 (35.9), 842 (20.3) [M]$^+$; 757 (17.3), 759 (44.4), 761 (28.5), [M−Br]$^+$); 557 (58.6), 559 (100), 561 (50.8).

Bis(5-{10-bromo-2,3-dihydronaphtho[2,3-*b*]-1,4-dioxinyl}(5-{2,3-dihydronaphtho[2,3-*b*]-1,4-dioxinyl}phosphane oxide (9): When aged NBS was used, formation of large quantities of **9** was observed, which was isolated by chromatography on neutral alumina column (hexane/AcOEt 7/3) as second fraction (yield 12%). M.p. 320–322°C (sint. 303°C); ^{1}H NMR (300 MHz, $CDCl_3$): δ=9.02 (d, ^3J(H,H)=8.67 Hz, 2H), 8.87 (d, ^3J(H,H)=8.50 Hz, 1H), 8.21 (d, ^3J(H,H)=8.49 Hz, 2H), 7.65 (d, ^3J(H,H)=8.19 Hz, 1H), 7.47–7.41 (m, 2H), 7.34–7.19 (m, 5H), 4.27–4.20 (m, 2H), 4.15–4.04 (m, 3H), 3.97–3.92 (m, 1H), 3.56–3.51 (m, 3H), 3.18–3.08 ppm (m, 3H); ^{31}P NMR (300 MHz, $CDCl_3$): δ=19.14 ppm (s); APT NMR (300 MHz; $CDCl_3$): δ=145.46 (d, ^2J(C,P)=3.62 Hz), 145.11 (d, ^2J(C,P)=3.62 Hz), 145.06 (d, ^2J(C,P)=3.32 Hz), 142.35 (d, ^3J(C,P)=11.02 Hz), 140.27 (d, ^3J(C,P)=2.79 Hz), 140.12 (d, ^3J(C,P)=2.41 Hz), 130.70–130.40 (3 overlapped d), 129.97 (d, ^3J(C,P)=11.77 Hz), 128.63 (d, ^3J(C,P)=11.02 Hz), 127.13 (s), 126.64 (d, ^3J(C,P)=5.51 Hz), 126.31 (d, ^4J(C,P)=2.26 Hz), 126.14 (d, ^3J(C,P)=5.21 Hz), 125.80–125.70 (m, 2 C), 125.21 (s), 124.57 (s), 118.14 (d, ^1J(C,P)=108.00 Hz), 117.94 (d, ^1J(C,P)=108.98 Hz), 116.58 (d, ^4J(C,P)=2.34 Hz), 112.24 (d, ^4J(C,P)=3.24 Hz), 112.20 (d, ^4J(C,P)=3.40 Hz), 64.48 (s), 63.66 (s), 63.39 (s), 63.12 ppm (s); MS (EI$^+$): *m/z* (%): 758 (30.5), 760 (62.4), 762 (33.9) [M+H]$^+$; 679 (28.1), 681 (32.9), [M+H]$^+$; 479 (98.3), 481 (100), 451 (41.0), 453 (39.7).

Chiral HPLC: HPLC enantioseparations and diastereoseparations were performed on stainless steel Chiralpak IC (250×4.6 mm I.D. and 250×10 mm I.D.; Chiral Technologies Europe, Illkirch, France) columns. All solvents for HPLC, synthesis, and spectral-grade solvents were purchased from Aldrich (Italy) and used without further purification. The analytical HPLC apparatus consisted of a PerkinElmer (Norwalk, CT, USA) 200 lc pump equipped with a Rheodyne (Cotati, CA, USA) injector, a 20 μL sample loop, a HPLC Dionex CC-100 oven (Sunnyvale, CA, USA), and a Jasco (Jasco, Tokyo, Japan) Model CD 2095 Plus UV/CD detector. For semipreparative separations a PerkinElmer 200 LC pump equipped with a Rheodyne injector, a 500 L sample loop, a PerkinElmer LC 101 oven, and Waters 484 detector (Waters Corporation, Milford, MA, USA) were used. The signal was acquired and processed by Clarity software (DataApex, Prague, The Czech Republic).

The mobile phase and the corresponding chromatographic data for each compound analyzed follow: **1a**: dichloromethane/methanol 100/1, k_1=0.83 (M_{res})-(−), α=1.35, R_s=2.95; **1**: dichloromethane/methanol 100/1, k_1=1.25 (M_{res})-(−), α=1.18, R_s=2.03; **3**: dichloromethane/methanol 100/1, k_1=0.80 (M_{res})-(−), α=1.35, R_s=2.74; **4**: dichloromethane/methanol 100/1, k_1=0.90 (M_{res})-(−), α=1.55, R_s=4.77; **5**: dichloromethane/methanol 100/1, k_1=1.11 (M_{res})-(−), α=1.86, R_s=5.16; **6**: dichloromethane/methanol 100/1, k_1=0.98 (M_{res})-(−), α=1.50, R_s=3.46; **7**: dichloromethane/methanol 100/1, k_1=0.97 (M_{res})-(−), α=1.27, R_s=3.09; **8**: dichloromethane/methanol 100/0.5, k_1=1.98 (M_{res})-(−), α=1.80, R_s=5.54; **9**: dichloromethane/methanol 100/1, k_1=0.55 (M_{res})-(−), α=1.69, R_s=3.09; **10**: *n*-hexane/dichloromethane/ethanol 20/100/1, k_1=1.15 (M_{res})-(−), α=1.88, R_s=6.09; **11**: Chiralpak IC/*n*-hexane-dichloromethane/ethanol 20/100/1, k_1=0.67 (M_{res})-(−), α=1.90, R_s=6.57. k_1 is the retention factor of the first-eluted enantiomer, defined as $(t_1-t_0)/t_0$, where t_0 is the column void time; α is the enantioselectivity factor, defined as k_2/k_1; R_s is the resolution factor, defined as $2(t_2-t_1)/(w_1+w_2)$ where t_1 and t_2 are retention times and w_1 and w_2 are band widths at the baseline in time units. Other chromatographic analytical conditions: flow rate, 1.0 mL min^{-1}; temperature, 25°C; detection: UV and CD at 254 or 280 nm (for **3**).

In off-column racemization studies, solutions of enantiomers of **1**, **3**–**9**, and **11** or diastereomers of **10** ($c\approx$0.1 mg mL^{-1}) were held at 55°C in chloroform contained in a closed vessel. The temperature was monitored by a Julabo (Julabo Labortechnik, Seelbach, Germany) Model HP-4 thermostat. Samples were withdrawn at fixed time intervals and analyzed by HPLC on a Chiralpak IC (250×4.6 mm I.D) column.

Polarimetry: Specific rotations were measured at 589 nm by a PerkinElmer polarimeter model 241 equipped with Na/Hg lamps. The volume of the cell was 1 mL and the optical path was 10 cm. The system was set at a temperature of 20°C.

Circular dichroism: The CD spectra were measured by using a Jasco Model J-700 spectropolarimeter. The optical path and temperature were set at 0.1 mm and 25°C. All CD spectra were recorded at a scan speed of 50 nm min^{-1} and spectral bandwidth of 1 nm. The spectra are averages computed over three instrumental scans and the intensities are presented in terms of specific ellipticity values (deg cm^2 dmol^{-1}).

Electrochemical measurements: Cyclovoltammetry was performed at scan rates of 0.02–1 V s^{-1} in HPLC-grade acetonitrile solutions at 0.00025–0.001 M concentration of each substrate, deaerated by N_2 bubbling, with 0.1 M tetrabutylammonium perchlorate (TBAP, Fluka) as supporting electrolyte at room temperature. The ohmic drop was compensated by the positive-feedback technique.[32] The experiments were carried out by using an AUTOLAB PGSTAT potentiostat (EcoChemie The Netherlands), run by a PC with GPES software. The glassy carbon working electrode (AMEL, surface area 0.071 cm^2) was cleaned with diamond powder (Aldrich, diameter 1 μm) on a wet cloth (STRUERS DP-NAP); the counterelectrode was a platinum disk; the reference electrode was an aqueous saturated calomel electrode, having in our working medium a difference of −0.385 V versus the Fc$^+$/Fc couple (the intersolvental redox potential reference currently recommended by IUPAC).[33]

Molecular modeling calculations: All molecular modeling calculations were performed on a PC equipped with 3.40 GHz Intel Pentium 4 CPU, 2 GB of RAM, and Windows 2000 Professional. Geometries of all phosphane oxides **1**–**11** and models **M0**, **M1**, and **M2** were optimized at the SCF level by the semiempirical AM1 method as implemented in SPARTAN 04 (Wavefunction, Inc., 18401 Von Karman Avenue, Suite 370, Irvine, CA 92612, USA). The structure of **1** was modeled according to the geometry elucidated by X-ray diffraction, that is, by orienting the naphthalene blades with the ethoxyl group *anti* to the P=O bond and respecting a C_3-symmetric disposition of the blades. The optimized structure of **1** was then used as starting geometry to model all other phosphane oxides, by merely performing suitable changes of groups substituting the blades and reoptimizing the thus-modified structures. Atomic charges employed as markers of the stereolability of phosphane oxides were computed according to the Mulliken procedure. Transition state (TS) structures of compounds **M0** and **6** were obtained in two steps. To attain the TS of **M0** a first geometry, relatively close to the TS involved in the M_0 mechanism, was obtained for **M0** by optimizing the structure with the three dihedral angles O-P-C_1-C_B constrained to 0°. Afterwards, the achieved structure, devoid of any constraint, was subjected to calculation of the TS, according to the procedure implemented in SPARTAN 04. The obtained TS was validated by the presence of only one imaginary frequency among the calculated vibrational modes. In the first step of the procedure carried out to obtain the TS of **6**, a starting geometry was modeled by reoptimizing the ground-state structure of **6** with the two dihedral angles O-P-C_1-C_B of 42.4 and 47.7° constrained to 0°. Afterwards, the obtained geometry was subjected to progressive variation of the remaining torsion from its initial values of 88.19° to the final one of −88.19°, again leaving the other two dihedral angles constrained to 0°. The structure lying on the maximum of the obtained potential energy profile was then submitted to the TS calculation without any constraint. The saddle-point state of the resulting structure was confirmed by calculation of the relevant vibrational modes (only one imaginary frequency was found).

Linear free-energy relationships: regression analyses: LFER analyses were based on the performance of linear regressions of sets of multiparameter equations [Eqs. (1S)–(6S) in the Supporting Information], each of which is expressed by the general structure reported in the text as Equa-

tion (1). With the aim of evaluating the casualness of the obtained correlations and quantifying the statistical weight of each used descriptor, the regression results were analyzed according to the well-known statistical F-test and T-test. Both linear regression analyses and statistical evaluations were performed by the dedicated mathematical functions implemented in Microsoft Office Excel 2003. Casualness was expressed through index F (probability distribution for two data sets by the function FDIST), and the significance of each descriptor of electronic effect by factors t_i, compared to the index T calculated through the Excel function TINV (inverse of the t-Student distribution). Probability related to the t-Student distribution in T-test was set as 0.1.

Crystal data: X-ray data of all structures were collected on two Bruker APEXII diffractometers with $Mo_{K\alpha}$ radiation ($\lambda = 0.71073$ Å) and graphite monochromator. The structures were solved by direct methods[34] and refined anisotropically by full-matrix least-squares techniques based on F^2. H atoms were in calculated positions with the exception of compound **11**, whose very good low temperature data allowed complete isotropic refinement.

*Tris[1-(2-methoxy)naphthyl]phosphane oxide (**1a**)*: $C_{33}H_{27}O_4P$, $M_r = 518.52$; trigonal, $R\bar{3}$; $a = 13.240(4)$, $c = 12.610(4)$ Å; $V = 1914.4(8)$ Å^3; room temperature; $Z = 3$; $\rho_{calcd} = 1.349$ g cm^{-3}; $\mu(Mo_{K\alpha}) = 0.147$ cm^{-1}; $F(000) = 816$; pink needle, $0.03 \times 0.04 \times 0.16$ mm; 4978 data collected, 978 unique, $R_{int} = 0.0662$, 495 with $I_o > 2\sigma(I_o)$. Small and poorly diffracting crystals. Attempts to collect data at low temperature failed, probably due to a phase transition. The final refinement was on 115 parameters and 1 restraint. The final results, on all and observed reflections, were $R_1 = 0.0987$ and 0.0361, $wR_2 = 0.0809$ and 0.0687, GOF 0.827; residues on the final map were from −0.14 to 0.11 e Å^{-3}. The absolute configuration was established by anomalous dispersion [Flack parameter = −0.001(19)]; due to the very high s.u. of the Flack parameters we are not sure that the refined absolute configuration is correct.

*Tris[1-(2-ethoxy-6-nitro)naphthyl]phosphane oxide (**3**)*: $C_{36}H_{30}N_3O_{10}P{\cdot}CH_2Cl_2$, $M_r = 780.53$; monoclinic, $C2/c$; $a = 19.353(3)$, $b = 12.901(2)$, $c = 29.834(4)$ Å; $\beta = 107.88(2)°$; $V = 7089.0(18)$ Å^3; $T = 123$ K; $Z = 8$; $\rho_{calcd} = 1.463$ g cm^{-3}; $\mu(Mo_{K\alpha}) = 0.293$ cm^{-1}; $F(000) = 3232$; yellow-brown block, $0.21 \times 0.30 \times 0.32$ mm; 35025 data collected, 8304 unique, $R_{int} = 0.0605$, 5614 with $I_o > 2\sigma(I_o)$. The final refinement was on 510 parameters and 37 restraints. The final results, on all and observed reflections, were $R_1 = 0.0679$ and 0.0429, $wR_2 = 0.1195$ and 0.1116, GOF 0.958; residues on the final map were from −0.38 to 1.18 e Å^{-3}. The dichloromethane molecule of solvation was disordered and was refined with soft restraints on C−Cl distances and Cl-C-Cl angles and also on the atomic displacement parameters.

*Tris[1-(2,6-diethoxy)naphthyl]phosphane oxide (**5**)*: $C_{42}H_{45}O_7P$, $M_r = 692.75$; triclinic, $P\bar{1}$; $a = 8.6357(10)$, $b = 14.829(2)$, $c = 15.589(2)$ Å; $\alpha = 63.023(13)$, $\beta = 78.012(14)$, $\gamma = 87.914(14)°$; $V = 1736.5(4)$ Å^3; $T = 103$ K; $Z = 2$; $\rho_{calcd} = 1.325$ g cm^{-3}; $\mu(Mo_{K\alpha}) = 0.132$ cm^{-1}; $F(000) = 736$; colorless triclinic parellelepiped, $0.12 \times 0.20 \times 0.23$ mm; 24165 data collected, 11474 unique, $R_{int} = 0.0492$, 7676 with $I_o > 2\sigma(I_o)$. The final refinement was on 451 parameters. The final results, on all and observed reflections, were $R_1 = 0.0779$ and 0.0474, $wR_2 = 0.1195$ and 0.1091, GOF 0.949; residues on the final map were from −0.35 to 1.09 e Å^{-3}. The higher residue was initially interpreted as a solvated water molecule with partial occupation. In the end, although the wR_2 index was about 1% lower, the occupation factor was only 0.08, and there were two short contacts with the ethyl H40C and H39A atoms (2.08–2.47 Å, respectively). This ethyl group has the largest anisotropic thermal parameters, probably due to the need to accommodate the solvated water and the consequent disorder. In the end we decided to ignore this residue and the possible partial presence of water.

*Bis[1-(2-ethoxy-6-nitro)naphthyl][1-(2-ethoxy-8-nitro)naphthyl]phosphane oxide (**6**)*: $C_{36}H_{30}O_{10}P{\cdot}1.85\,CHCl_3$, $M_r = 917.20$; monoclinic, $P2_1$; $a = 8.8385(5)$, $b = 15.8036(11)$, $c = 14.9548(10)$ Å; $\beta = 91.277(2)°$; $V = 2088.4(2)$ Å^3; room temperature; $Z = 2$, $\rho_{calcd} = 1.459$ g cm^{-3}; $\mu(Mo_{K\alpha}) = 0.481$ cm^{-1}; $F(000) = 939$; colorless block, $0.08 \times 0.22 \times 0.48$ mm; 24477 data collected, 4030 unique, $R_{int} = 0.0704$, 3198 with $I_o > 2\sigma(I_o)$. The crystals diffract very poorly, and slowly lose solvent of crystallization. An attempt to collect data at low temperature failed, because the diffraction data got worse, probably due to a phase transition. To avoid the decay due to solvent loss, the crystal used in fast data collection was completely covered by glue. The final refinement was on 528 parameters and 1 restraint. The final results, on all and observed reflections, were $R_1 = 0.0575$ and 0.0407, $wR_2 = 0.1110$ and 0.1049, GOF 0.994; residues on the final map were from −0.18 to 0.21 e Å^{-3}. The quality of data and their resolution were very low. We refined both the Flack index and the population factors of the two independent molecules of solvated chloroform; the latter converged at about 0.96 and 0.90. In spite of the low data/parameters ratio we are confident that the found absolute configuration is correct.

*Tris[4-(2,2-dimethyl-naphtho[2,3-d]-1,3-dioxolyl)]phosphane oxide (**11**)*: $C_{39}H_{33}O_7P$, $M_r = 644.62$; trigonal, $R\bar{3}$; $a = 11.5060(12)$, $c = 21.052(2)$ Å; $V = 2413.6(4)$ Å^3; $T = 123$ K; $Z = 3$; $\rho_{calcd} = 1.330$ g cm^{-3}; $\mu(Mo_{K\alpha}) = 0.138$ cm^{-1}; $F(000) = 1014$; colorless triclinic parallelepiped, $0.18 \times 0.36 \times 0.42$ mm; 6920 data collected, 3135 unique, $R_{int} = 0.0257$, 2966 with $I_o > 2\sigma(I_o)$. The final refinement was on 186 parameters and 1 restraint. The final results, on all and observed reflections, were $R_1 = 0.0332$ and 0.0298, $wR_2 = 0.0788$ and 0.0761, GOF 1.048; residues on the final map were from −0.20 to 0.32 e Å^{-3}.

CCDC-864258 (**11**), CCDC-864259 (**1a**), CCDC-864260 (**3**), CCDC-864261 (**5**) and CCDC-864262 (**6**) contain the supplementary crystallographic data for this paper. These data can be obtained free of charge from The Cambridge Crystallographic Data Centre via www.ccdc.cam.ac.uk/data_request/cif.

Acknowledgements

Work supported by MIUR PRIN-2007 *"Catalizzatori innovativi a base di metalli di transizione per sintesi mirate chemo- e stereo-selettive"*, by CNR and, in part, by Laboratori Alchemia s.r.l.; T. B. thanks the Dipartimento di Chimica Organica e Industriale of the University of Milano for hospitality.

[1] a) G. Haberhauer, S. Ernst, C. Wilch, *Chem. Eur. J.* **2011**, *17*, 8643; b) H. Ito, T. Abe, K. Saigo, *Angew. Chem.* **2011**, *123*, 7282; *Angew. Chem. Int. Ed.* **2011**, *50*, 7144; c) I. Alkorta, J. Elguero, *Tetrahedron: Asymmetry* **2010**, *21*, 437; d) Á. Pintér, G. Haberhauer, I. Hyla-Kryspin, S. Grimme, *Chem. Commun.* **2007**, 3711; e) C. Bolm, W. M. Davis, R. L. Halterman, K. B. Sharpless, *Angew. Chem.* **1988**, *100*, 882; *Angew. Chem. Int. Ed. Engl.* **1988**, *27*, 835.

[2] a) P. Finocchiaro, D. Gust, K. Mislow, *J. Am. Chem. Soc.* **1973**, *95*, 8172; b) P. Finocchiaro, D. Gust, K. Mislow, *J. Am. Chem. Soc.* **1974**, *96*, 2165; c) J. D. Andose, K. Mislow, *J. Am. Chem. Soc.* **1974**, *96*, 2168; d) P. Finocchiaro, D. Gust, K. Mislow, *J. Am. Chem. Soc.* **1974**, *96*, 2176; e) P. Finocchiaro, D. Gust, K. Mislow, *J. Am. Chem. Soc.* **1974**, *96*, 3198; f) P. Finocchiaro, D. Gust, K. Mislow, *J. Am. Chem. Soc.* **1974**, *96*, 3205; g) C. Foces-Foces, F. H. Cano, M. Martínez Ripoll, R. Faure, C. Roussel, R. M. Claramunt, C. López, D. Sanz, J. Elguero, *Tetrahedron: Asymmetry* **1990**, *1*, 65.

[3] R. Glaser, J. F. Blount, K. Mislow, *J. Am. Chem. Soc.* **1980**, *102*, 2777.

[4] K. Mislow, *Acc. Chem. Res.* **1976**, *9*, 26.

[5] T. Benincori, G. Celentano, T. Pilati, A. Ponti, S. Rizzo, F. Sannicolò, *Angew. Chem.* **2006**, *118*, 6339; *Angew. Chem. Int. Ed.* **2006**, *45*, 6193.

[6] T. Benincori, A. Marchesi, T. Pilati, A. Ponti, S. Rizzo, F. Sannicolò, *Chem. Eur. J.* **2009**, *15*, 86.

[7] a) T. Benincori, A. Marchesi, P. R. Mussini, T. Pilati, A. Ponti, S. Rizzo, F. Sannicolò, *Chem. Eur. J.* **2009**, *15*, 94; b) C. Qin, H. Wu, J. Cheng, X. Chen, M. Liu, W. Zhang, W. Su, J. Ding, *J. Org. Chem.* **2007**, *72*, 4102; c) C. Qin, J. Chen, H. Wu, J. Cheng, Q. Zhang, B. Zuo, W. Su, J. Ding, *Tetrahedron Lett.* **2008**, *49*, 1884; d) T. Shimada, K. Mukaide, A. Shinohara, J. W. Han, T. Hayashi, *J. Am. Chem. Soc.* **2002**, *124*, 1584.

[8] The synthesis and characterization of the phosphanes corresponding to the phosphane oxides **1a**, **2**, **5**, **10**, and **11** are described in the article immediately following this one. S. Rizzo, T. Benincori, V. Bonometti, R. Cirilli, P. R. Mussini, M. Pierini, T. Pilati, F. Sannicolò, *Chem. Eur. J.* DOI: 10.1002/chem.201201182.
[9] a) T. Zhang, D. Nguyen, P. Franco, Y. Isobe, T. Michishita, T. Murakami, *J. Pharm. Biomed. Anal.* **2008**, *46*, 882; b) R. Ferretti, B. Gallinella, F. La Torre, L. Zanitti, L. Turchetto, A. Mosca, R. Cirilli, *J. Chromatogr. A* **2009**, *1216*, 5385.
[10] G. Angelini, C. Coletti, P. De Maria, R. Ballini, C. Gasbarri, A. Fontana, M. Pierini, G. Siani, *J. Org. Chem.* **2012**, *77*, 899–907.
[11] A. Ciogli, A. Fontana, F. Gasparrini, M. Maggini, M. Giovannoli, M. Pierini, F. Busolo, G. Siani, C. Villani, *Eur. J. Org. Chem.* **2012**, 193.
[12] M. J. Citra, *Chemosphere* **1999**, *38*, 191.
[13] S. Jelfs, P. Ertl, P. Selzer, *J. Chem. Inf. Model.* **2007**, *47*, 450.
[14] J. Zhang, T. Kleinoder, J. Gasteiger, *J. Chem. Inf. Model.* **2006**, *46*, 2256.
[15] G. Angelini, P. De Maria, A. Fontana, M. Pierini, G. Siani, *J. Org. Chem.* **2007**, *72*, 4039.
[16] R. Cirilli, R. Costi, R. Di Santo, F. Gasparrini, F. La Torre, M. Pierini, G. Siani, *Chirality* **2009**, *21*, 24–34.
[17] A. Fontana, P. De Maria, G. Siani, M. Pierini, S. Cerritelli, R. Ballini, *Eur. J. Org. Chem.* **2000**, 1641.
[18] S. L. Dixon, P. C. Jurs, *J. Comput. Chem.* **1993**, *14*, 1460.
[19] W. Cabri, I. D′Acquarica, P. Simone, M. Di Iorio, M. Di Mattia, F. Gasparrini, F. Giorgi, A. Mazzanti, M. Pierini, M. Quaglia, C. Villani, *J. Org. Chem.* **2011**, *76*, 1751.
[20] T. N. Brown, N. Mora-Diez, *J. Phys. Chem. B* **2006**, *110*, 20546.
[21] M. C. Rezende, *Tetrahedron* **2001**, *57*, 5923.
[22] M. C. Rezende, *J. Braz. Chem. Soc.* **2001**, *12*, 73.
[23] R. R. Contreras, P. Fuentealba, M. Galva'n, P. Pérez, *Chem. Phys. Lett.* **1999**, *304*, 405.
[24] F. Méndez, M. L. Romero, F. De Proft, P. Geerlings, *J. Org. Chem.* **1998**, *63*, 5774.
[25] W. Yang, W. J. Mortier, *J. Am. Chem. Soc.* **1986**, *108*, 5708.
[26] C. Hansch, A. Leo, R. W. Taft, *Chem. Rev.* **1991**, *91*, 165.
[27] V. Le Berre, L. Angély, N. Simonet-Guéguen, J. Simonet, *J. Chem. Soc. Chem. Commun.* **1987**, 984.
[28] S. Besbes-Hentati, H. Said, M. Bouvet, *Electrochim. Acta* **2007**, *52*, 4715, and references therein.
[29] S. Besbes-Hentati, H. Said, *Electrochim. Acta* **2010**, *55*, 5636 and references therein.
[30] J.-M. Saveant, S. K. Binh, *J. Electroanal. Chem.* **1978**, *88*, 27.
[31] A. J. Bard, L. R. Faulkner, *Electrochemical Methods. Fundamentals and Applications*, Wiley, New York, **2002**, pp. 648–650.
[32] a) G. Gritzner, J. Kuta, *Pure Appl. Chem.* **1984**, *56*, 461; b) G. Gritzner, *Pure Appl. Chem.* **1990**, *62*, 1839.
[33] M. C. Burla, M. Camalli, B. Carrozzini, G. L. Cascarano, C. Giacovazzo, G. Polidori, R. Spagna, *J. Appl. Crystallogr.* **2003**, *36*, 1103.
[34] G. M. Sheldrick, *Acta Crystallogr. A* **2008**, *64*, 112–122.

Received: April 6, 2012
Revised: August 2, 2012
Published online: ■■ ■■, 0000

Residual Stereoisomerism

T. Benincori, V. Bonometti, R. Cirilli, P. R. Mussini, A. Marchesi, M. Pierini, T. Pilati, S. Rizzo, F. Sannicolò** ..... ▮▮▮▮–▮▮▮▮

Steric and Electronic Effects on the Configurational Stability of Residual Chiral Phosphorus-Centered Three-Bladed Propellers: Tris-aryl Phosphane Oxides

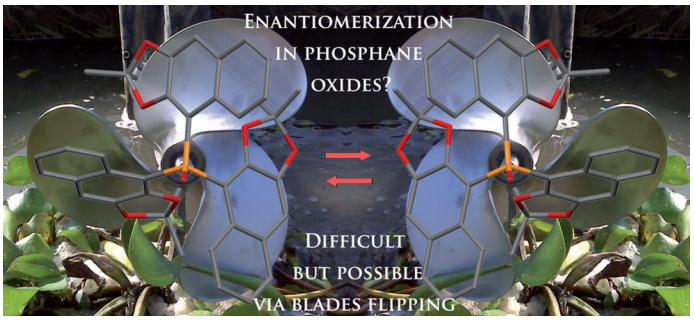

Residual stereoisomers of tris-aryl phosphane oxides, which can be regarded as phosphorus-centered three-bladed propellers (see figure), were isolated in a stereochemically pure state and found to be highly configurationally stable at room temperature (stereoisomerization barriers of about 27 kcal mol^{-1}). The chiroptical properties of the residual stereoisomers and the assignments of absolute configuration are discussed. The configurational stability was found to be scarcely influenced by the electronic properties of the substituents on the aromatic rings constituting the blades, whereas steric effects play the most relevant role.

